CHALMERS

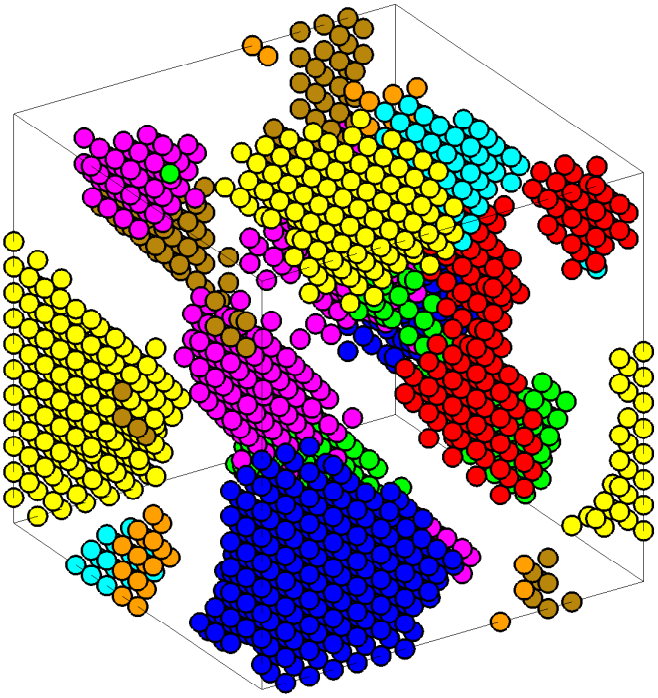

Local and Global Ordering in Barium Zirconate, a Model Potential Study

Master's Thesis in Applied Physics

ERIK FRANSSON,
JOHANNES LAURELL HÅKANSSON

Department of Applied Physics
Division of Materials and Surface Theory
Chalmers University of Technology
Gothenburg, Sweden 2014

This page is intentionally left blank.

Thesis for the degree of Master of Science in Engineering Physics

Local and Global Ordering in Barium Zirconate, a Model Potential Study

ERIK FRANSSON,
JOHANNES LAURELL HÅKANSSON

CHALMERS

Department of Applied Physics
Division of Materials and Surface Theory
Chalmers University of Technology
Gothenburg, Sweden 2014

Local and Global Ordering in Barium Zirconate, a Model Potential Study

ERIK FRANSSON, JOHANNES LAURELL HÅKANSSON

Department of Applied Physics
Division of Materials and Surface Theory
Chalmers University of Technology
SE-412 96 Gothenburg
Sweden
Telephone: +46 (0)31-772 1000

Cover:
Clusters of different distortion phases in $BaZrO_3$.

Chalmers Reproservice
Gothenburg, Sweden 2014

Local and Global Ordering in Barium Zirconate, a Model Potential Study
Erik Fransson, Johannes Laurell Håkansson
Department of Applied Physics
Chalmers University of Technology, Gothenburg 2014

Abstract

Barium zirconate ($BaZrO_3$) is a promising candidate as proton conducting electrolyte to be be used in fuel cells. Despite extensive investigations the basic structure of $BaZrO_3$ as a function of temperature is not fully understood. It is related to possible instabilities in the cubic system that may show up in the local and/or global ordering of the material as a function of temperature.

In this study three different types of simple models for barium zirconate are created, one giving rise to an ordinary cubic structure, one giving rise to distortion and one intermediate on the limit between the two others. All three models are based on a pair potential taking three types of interaction into account, Pauli repulsion, van der Waals interaction and Coulomb interaction. Static and dynamic properties obtained from computer simulations of the three models are presented to illustrate the different behaviours.

The stability of the models are investigated by calculating phonon spectra. Molecular dynamics are used to study the time evolution of the system. The oxygen atoms for the model giving rise to distortion are found to move a lot more compared to the other two models due to the potential being softer around the ideal cubic perovskite. The obtained radial distribution function indicate that the distortions are not found for temperatures above 300 K, meaning a phase transition happens. Furthermore for large systems the formation of clusters of different distortions are observed.

Using the type of simple models created one could in an easy way compare experimental results with computer simulations to get a better understanding of instabilities in perovskites in general and barium zirconate in particular.

Keywords: Barium zirconate, Perovskite structure, Molecular dynamics, Model potentials

This page is unintentionally left blank.

Acknowledgements

We would like to express our gratitude to our supervisor, professor Göran Wahnström, for suggesting and guiding us through this thesis. We would also like to thank Martin Petisme and Anders Lindman for their support with the computer simulations. In addition Karl Larsson and Johan Alvbring at Chalmers Centre for Computational Science and Engineering (C3SE) are acknowledged for assistance concerning technical and implementation aspects in making the code run on the C3SE resources.

Furthermore we would like to thank Joakim Löfgren and Erik Jedvik for all the help and interesting discussions throughout this project. Their parallel Master's theses regarding barium zirconate have been very fruitful for our work. A thanks also goes to Mattias Ångqvist, Johan Lövgren, Simon Andersson, Adam Arvidsson and Jakob Billemar for accompanying us during fika breaks and helping us with the final touch on this report. Last, but not least, we would like to send a thank you to all the others that in some way have contributed to the completion of this thesis.

Göteborg, Ascension Day 2014

The Authors

This page would be blank if I were not here telling you that this page would be blank if I were not here telling you that ...

Contents

1

Introduction

The last couple of years there has been an increasing awareness of the effect humanity has on the nature and climate. The will to replace fossil fuels with green energy alternatives has led to an increasing interest in fuel cells. There are many different types of fuel cells but they all consist of an anode, a cathode and an electrolyte. One promising electrolyte for the proton conducting fuel cell is barium zirconate ($BaZrO_3$).

Although a lot of research about $BaZrO_3$ has been done the basic structure of the material as a function of temperature is not fully understood. It is related to possible instabilities in the cubic system that may show up in the local and/or global ordering of the material as function of temperature.

1.1 Purpose and limitations

The intention of this study was to find three different types of simple potentials describing barium zirconate ($BaZrO_3$), one giving rise to an ordinary cubic structure, one giving rise to distortion and one intermediate on the limit between the two others. In order to distinguish them from each other in an easy way they are called model A (stable), model B (intermediate) and model C (unstable) throughout the report.

To test if the models give rise to distortion phonon spectra were calculated based on the simple potentials. Molecular dynamics simulations were then performed in order to study both static and dynamic properties of the models as a function of temperature.

The aim of this project is to do qualitative rather than quantitative research. There is thus no intention to make exact predictions about the properties of barium

zirconate. The whole study is carried out using computer simulations, no experimental measurements are done.

1.2 Thesis outline

This thesis contains seven chapters. The chapter following the introduction, Barium zirconate, is a more in depth introduction to the material barium zirconate ($BaZrO_3$) and the structural family of perovskites which $BaZrO_3$ is part of. Some properties of the perovskite structure and $BaZrO_3$ are described and in the final section of the chapter a brief review about previous research on the subject is given.

The third chapter consists of a collection of the basic theory used in the thesis. It is written in a detached way to make it easy to use as a reference when reading the other parts of the report. Examples of theory that is described in this chapter is pair potential (3.2) and mean square displacement (3.5).

In the fourth chapter, Computational methods, the practical details about the model used and how the simulations were done is described. This chapter includes a section about molecular dynamics (4.2) and sections about software that was used (4.4 and 4.5). An example of code that was used can be found in appendix A.

In chapter 5 the obtained results are presented. Chapter 6 contains a discussion of the obtained results and an outlook on possible future studies and finally chapter 7 is a conclusion of the thesis.

2

Barium zirconate

In this chapter the material studied in this project, barium zirconate ($BaZrO_3$), is presented in more detail. In section 2.1 a brief description of the structural family of perovskites, which $BaZrO_3$ is part of, is made. The last part of this chapter, section 2.2, is a brief review of some results obtained in previous studies about barium zirconate.

2.1 Perovskites

A material is said to have a perovskite structure if it has the same crystal structure as the mineral perovskite, i.e calcium titanate or calcium titanium oxide ($CaTiO_3$). The general chemical formula for a perovskite structure can be written as ABX_3 where A and B represent cations of different sizes, the A atoms being larger, and X is an anion. In the ideal cubic structure each B cation is surrounded by an octahedron of the anions X with the A cation located in the middle of the cube created by eight octahedrons. An illustration of this can be seen in figure 2.1. As seen the perovskite structure is in principle a superposition of a bcc lattice and an fcc lattice.

Most materials with the perovskite structure are distorted in some way, so also the mineral perovskite itself. As an estimate of the tendency for distortion to occur in a perovskite the Goldschmidt tolerance factor has been introduced. To classify different kinds of distortions the so called Glazer notation is often used.

2.1.1 Tolerance factor

As mentioned the general chemical formula for a perovskite structure can be written as ABX_3. For a cubic system the lattice constant is given by (2.1).

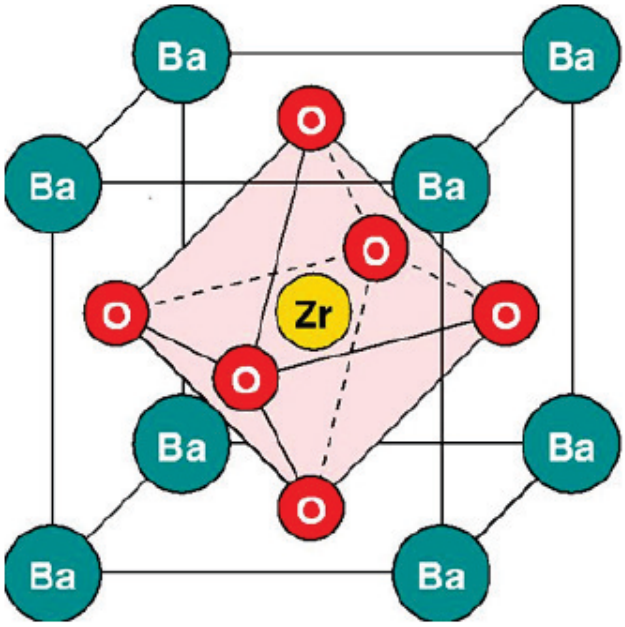

Figure 2.1: +Fixa egen bild+ The structure of barium zirconate ($BaZrO_3$) with a zirconium atom surrounded by an octahedron of oxygen atoms.

$$a = \sqrt{2}(r_A + r_X) = 2(r_B + r_X) \tag{2.1}$$

where r_A, r_B and r_X are ionic radii. The Goldschmidt tolerance factor, t, is the ratio between the two expressions for a and is defined according to equation (2.2). It is used to predict lattice distortions in perovskite structures [1].

$$t = \frac{r_A + r_X}{\sqrt{2}(r_B + r_X)} \tag{2.2}$$

An ideal cubic perovskite corresponds to $t = 1$. If either the B ion is too large or the A ion too small t becomes less than unity and the lattice distorts by the BX_6 octahedra tilting in order to fill space. For t larger than one hexagonal variants of the perovskite structure are stable. In reality perovskites are not perfectly ionic and since the tolerance factor is based on the ionic radius it should thus only be used as an rough estimate.

2.1.2 Glazer notation

To construct a general classification describing the tilt of the BX_6 octahedron in a perovskite structure one can consider all tilts as combinations of component tilts about the three tetrad axes. The final tilt arrangement will then depend on the order in which

the tilt operations are carried out. For small angles however this dependence will only be of second order.

For small angles of tilt the component tilts can be taken to be about the pseudocubic axes prior to tilting. The magnitude of each component tilt can then be described by a set of three letters which refer to the axes in the order [100], [010], [001], and which in the general case of unequal tilts are denoted *abc* [2]. This way of describing tilts was originally developed by Glazer and is often referred to as Glazer's notation or as in this report Glazer notation [3].

In Glazer notation equality of tilts is denoted by repeating the same letter, e.g. *aac* means equal tilt about [100] and [010] with a different tilt about [001] and *aaa* indicates that the tilt about all three axes are equal in magnitude.

When a single octahedron in a perovskite structure is tilted the neighbouring octahedron will also have to tilt in order to not completely deform the original structure. This is due to the fact that each oxygen atom in an octahedra is also part of a neighbouring octahedra. One thus has that for any tilt axis successive octahedra in directions perpendicular to it will have opposite tilt about that axis. Successive octahedra along an axis can however have either the same or the opposite sense of tilt. In order to the describe this the Glazer notation also includes superscripts +, - or 0 for each letter indicating whether successive octahedra along an axis have the same tilt, opposite tilt or no tilt about that axis.

Using the Glazer notation then for example the tilt $a^-a^-a^-$ indicates an equal tilt about each of the three axes corresponding to a rotation vector $\vec{\omega} = (\pm 1, \pm 1, \pm 1)$. The three minuses in the notation indicate that the tilt is alternating in all three directions. This means that the octahedrons in neighbouring cells to one with rotation vector $\vec{\omega}$ will have a distortion corresponding to a rotation vector $-\vec{\omega}$ while the next nearest neighbours will have the same rotation vector and so on.

2.2 Previous studies

Due to its special properties and many applications in modern technology the family of perovskite structures has been subject for numerous studies. Despite the many studies of barium zirconate, often including dopants, the detailed features of both the short-range and long-range crystal structure are yet to be fully explained.

In a study published 1995 Zhong and Vanderbilt obtained the stiffness k^R of R-point antiferrodistortive (AFD) phonon mode, i.e. alternating distortions in all directions, and the tolerance factor t for eight perovskites [4]. This result is reproduced in table 2.1.

From the table Zhong and Vanderbilt conclude that $BaTiO_3$ and $KNbO_3$ are clearly stable with respect to AFD distortion which is consistent with experiments. The last

Table 2.1: Stiffness k^R of R-point AFD phonon mode (in Hartree) and tolerance factor t for several perovskite compounds obtained in a previous study [4].

	k^R	t		k^R	t
$BaTiO_3$	0.295	1.07	$SrTiO_3$	-0.042	1.01
$KNbO_3$	0.242	1.06	$NaNbO_3$	-0.133	0.97
$BaZrO_3$	-0.021	1.01	$PbZrO_3$	-0.324	0.97
$PbTiO_3$	-0.037	1.03	$CaTiO_3$	-0.375	0.97

three compunds in the table, $CaTiO_3$, $PbZrO_3$ and $NaNbO_3$, were found to have a strong AFD instability. For $SrTiO_3$, $PbTiO_3$ and $BaZrO_3$ calculations show a weak AFD instability. Both $SrTiO_3$ and $PbTiO_3$ have been observed to have weak phase transitions at $T = 105\,\mathrm{K}$ and $T = 180\,\mathrm{K}$ respectively while it is stated that $BaZrO_3$ is observed to remain cubic down to $T = 0$. To explain the behaviour of $BaZrO_3$ it is suggested that the weak instability found in the calculations could be suppressed by quantum zero-point fluctuations.

In many studies the phonon spectrum for barium zirconate has been calculated using density functional theory (DFT) [5] [6] [7]. Using local-density approximation (LDA) the results have shown that $BaZrO_3$ is unstable. An example of this is reproduced in figure 2.2 where imaginary modes (illustrated as negative) indicate that the structure is unstable. In some DFT calculations using generalized gradient approximation (GGA) the undistorted perovskite structure is however found to be stable as seen in figure 2.3. To obtain this spectrum PBE, a version of GGA, was used and the difference compared to figure 2.2 is quite clear, especially at the R-point where there are unstable modes only in the latter case.

The studies based on first-principles calculations are as seen not unequivocal. This is also the case for experimental research, the picture is not entirely clear for barium zirconate. In an article by Akbarzadeh et al. published 2005 experimental results validating the cubic perovskite structure for $BaZrO_3$ down to $T = 2\,\mathrm{K}$ are presented [7]. It is concluded that there is no long-range-order phase transition. However on the basis of first-principles calculations (phonon spectrum obtained with DFT) it is suggested that the experimentally observed dielectric anomalies at the lowest temperatures (about 15 K) might arise from local rotation of the oxygen octahedra. Anomalies at somewhat higher temperatures (about 50 K) are instead proposed to be caused by defects in the material, like oxygen vacancies, and/or unavoidable impurity ions, like Fe^{3+}.

In an experimental study by Giannici et al. published 2011 measurements at 25 K was performed for both undoped $BaZrO_3$ and yttrium-doped $BaZrO_3$ [8]. In the article it is stated that there is no doubt about $BaZrO_3$ being a cubic perovskite on a long-range scale while there are indications that some local distortions occur. Due to thermal parameters indicating a larger distortion than expected for a cubic perovskite incoherent and/or

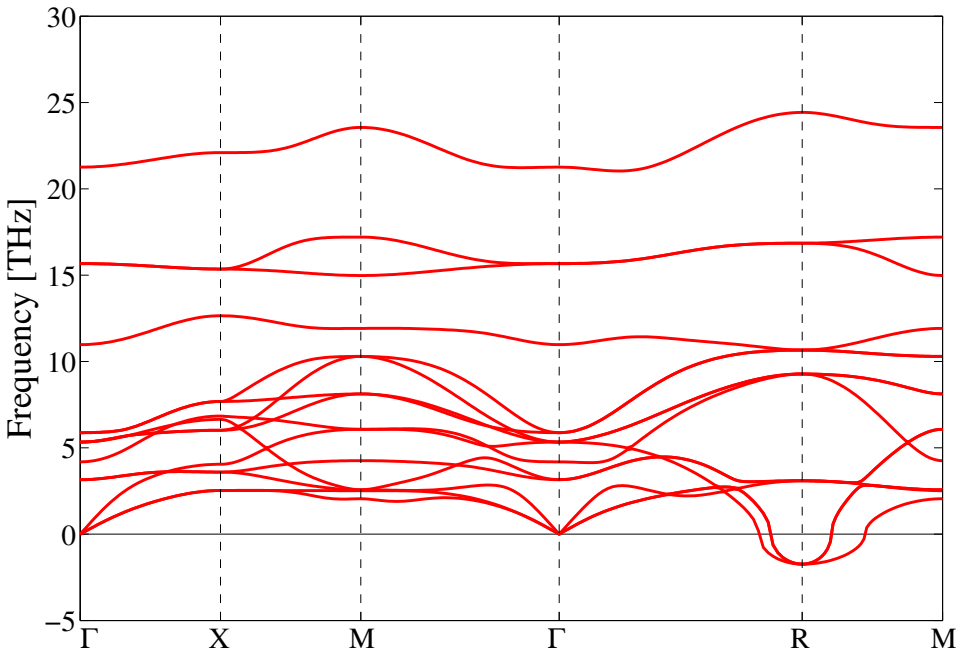

Figure 2.2: Phonon spectrum for barium zirconate ($BaZrO_3$) obtained using DFT with LDA. This spectrum is, with permission, reproduced from data obtained by Erik Jedvik ++ev cite++

transient local deviations from the cubic symmetry is proposed. For yttrium-doped $BaZrO_3$ obtained results are suggested to arise from tilting of theYO_6 octahedra.

Research combining first principle calculations (phonon spectrum obtained with DFT) and experimental measurements were published by Lebedev and Sluchinskaya in an article 2013 [5]. For $T = 300\,\mathrm{K}$ results have been obtained that indicate rotational vibrations of the oxygen octahedra. Based on the theoretical calculations it is proposed that the absence of the long-range order in $BaZrO_3$ at low temperatures is due to a structural glass state being formed upon cooling. Phases with different octahedral rotations at different points of the sample then altogether give rise to the absence of long-range order. Lebedev and Sluchinskaya also support this hypothesis with their calculations that show a relatively small energy difference between different tilts of the oxygen octahedra.

In an article published in March 2014 Yang et al. presents results from an experimental study of the high pressure behaviour of $BaZrO_3$ at room temperature [9]. A phase transition from cubic phase to tetragonal phase were found to take place at 17.2 GPa. This is suggested to arise from the rotational instability of the oxygen octahedra in accordance with the unstable phonon modes.

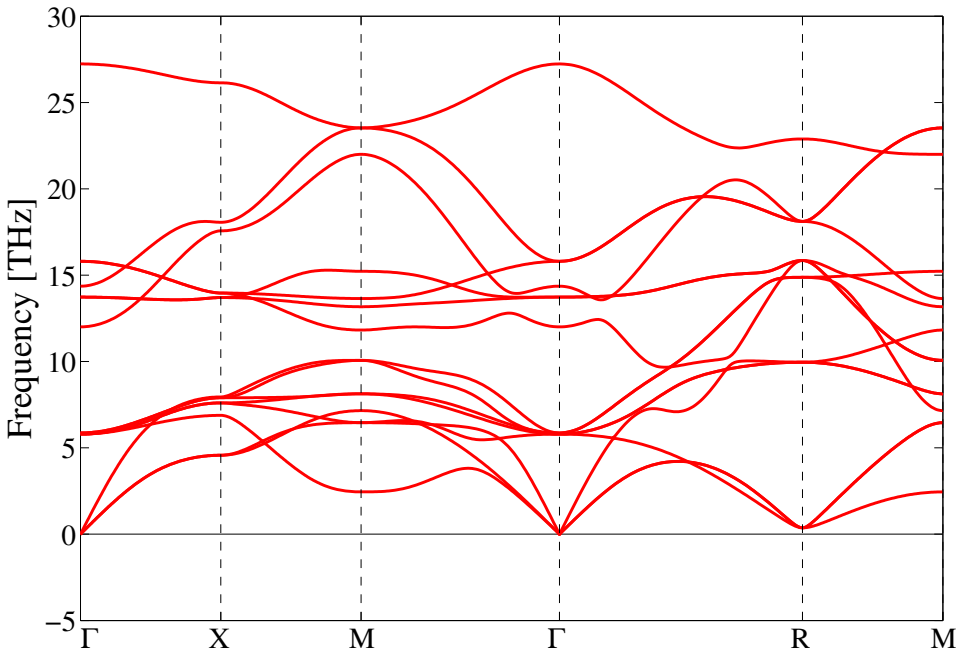

Figure 2.3: Phonon spectrum for barium zirconate ($BaZrO_3$) obtained using DFT with GGA. This spectrum is, with permission, reproduced from data obtained by Erik Jedvik ++ev cite++

To sum it all up previous studies are consistent in the sense that more studies are needed in order to get a satisfactory understanding of the short-range and long-range crystal structure of barium zirconate.

3

Theory

In this chapter some of the basic theory used in the study is presented. It is written in a detached way for ease of reading. The experienced reader can skim through it while it will be useful for the novice reader to read the whole chapter more carefully. Regardless of previous knowledge this section will hopefully be a practical reference when reading later parts of the thesis

For a more thorough description of the subjects treated in this chapter refer to the sources cited or to a textbook in the field of condensed matter physics such as *Introduction To Solid State Physics* by Charles Kittel.

3.1 Phonons

For a periodic system the phonon frequencies for a wave vector $\mathbf{k}$ are given by the eigenvalues of the Dynamical matrix D defined as

$$D_{s\alpha,t\beta}(\mathbf{k}) = \frac{1}{\sqrt{M_s M_t}} \sum_i \Phi_{is\alpha,jt\beta} \exp[i\mathbf{k} \cdot (\mathbf{R}_j + \boldsymbol{\tau}_t - \mathbf{R}_i - \boldsymbol{\tau}_s)] \tag{3.1}$$

where α and β are Cartesian directions, s and t are atoms, M is mass for an atom, i and j are primitive cells, R are vectors connecting primitive cells, τ are vectors which define the atomic positions in the cells and $\Phi_{is\alpha,jt\beta}$ is the so called force-constant matrix.

The force-constant matrix, $\Phi_{is\alpha,jt\beta}$, is defined as the second derivative of energy with respect to displacements of atoms from their equilibrium positions, i.e.

$$\Phi_{is\alpha,jt\beta} = \frac{\partial^2 U}{\partial u_{is\alpha} \partial u_j t\beta} \tag{3.2}$$

where $\mathbf{u}$ is a displacement vector of atom s, in cell i (or atom t in cell j).

Using the definition of the Dynamical matrix (3.1) and assuming that the motion of the ions are sinusoidal in time one could deduce an eigenvalue equation for the angular frequency given by equation (3.3) [10]

$$\mathbf{D}(\mathbf{k}) \cdot \mathbf{u} = \omega^2 \mathbf{u} \tag{3.3}$$

where $\mathbf{u}$ is the eigenvector. The displacement of an atom s in a primitive cell i in direction α is denoted $S_{is\alpha}$ and given by equation (3.4).

$$S_{is\alpha} = \frac{1}{\sqrt{M_s}} u_{s\alpha} \mathrm{e}^{i\mathbf{k}\cdot\mathbf{R_i}} \tag{3.4}$$

where $u_{s\alpha}$ is the element of $\mathbf{u}$ representing the direction α for atom s. Negative eigenvalues of the dynamical matrix, corresponding to imaginary phonon frequencies, suggests that the system is unstable with respect to moving the atoms according to equation (3.4) [5].

In this study the so-called small displacement method is used to obtain the phonon spectrum. With this method the force-constant matrix is, based on equation (3.2), calculated as minus the numerical derivative of the forces induced by displacing once at a time all the atoms of the lattice along the three Cartesian components [11].

3.2 Pair potential

There are many different kind of models for studying materials in computer simulations. In general however a system consisting of N atoms can be described by a potential depending on the position of each individual atom

$$V = V(\mathbf{r}_1,\mathbf{r}_2,...,\mathbf{r}_{N-1},\mathbf{r}_N) \tag{3.5}$$

In this study a so called pair potential has been used for all the simulations. A pair potential, where one assumes that all interatomic interactions are pairwise additive, is the simplest form of potential. The total potential energy for a system consisting of N atoms is then given by

$$V = \sum_{i=1}^{N} \sum_{j>i}^{N} v_{ij}(r_{ij}) \tag{3.6}$$

where v_{ij} is the interaction energy between atom i and atom j and $r_{ij} = |\mathbf{r_i} - \mathbf{r_j}|$ is the distance between those atoms.

In order to get meaningful results using a pair potential the atoms in the system to be studied should not share any electrons. This is the case for e.g. noble gases and ionic systems (like $BaZrO_3$) and in those cases a pair potential could be favorable due

to its simplicity. For more complicated systems one will need more complicated models to get any useful results. A widely used method is density functional theory (DFT) which often computes very accurate results. DFT is however very computationally expensive compared to using a simple pair potential. This means that with a pair potential simulations consisting of millions of atoms can be performed which simply is not possible with DFT.

3.2.1 Buckingham potential and Coulomb interaction

In this study three types of interaction were taken into account, Pauli repulsion, van der Waals interaction and Coulomb interaction. The Buckingham potential, given by equation (3.7), were used to describe the Pauli repulsion and the van der Waals interaction.

$$U^{buck}(r_{ij}) = A_{ij}e^{-r_{ij}/\rho_{ij}} - \frac{C_{ij}}{r_{ij}^6} \tag{3.7}$$

In the equation r_{ij} is the distance between atom i and j. The parameters A_{ij}, ρ_{ij} and C_{ij} are empirically adapted based on the system to be studied. In principle one could use parameters suitable for each separate pair but in order to fit with experimental data for the whole system small adjustments are often necessary. Adding Coulombs law to the Buckingham potential the total interaction energy between two atoms becomes

$$U(r_{ij}) = A_{ij}e^{-r_{ij}/\rho_{ij}} - \frac{C_{ij}}{r_{ij}^6} + \frac{q_i q_j}{r_{ij}} \tag{3.8}$$

where q_i is the charge of atom i.

3.3 Ewald summation

The first two terms in the pair potential given by equation (3.8) are short ranged, i.e. they decay rapidly as r_{ij} grows, and are therefore negligible for large r_{ij}. The Coulombic term however is long ranged and can not be neglected for large r_{ij}. For a large number of charged particles this term becomes computationally expensive due to the amount of pairs i,j that contributes to the energy.

Ewald summation is a way to handle the Coulombic interaction in a computationally efficient way when the number of charged particle is large [12]. The basic idea of the method is to divide the summation of interaction energies into a summation in real space and a summation in reciprocal space (Fourier space). The resulting expression for the

Coulomb interaction is given by

$$\begin{aligned} U_{Ewald} &= \frac{1}{2}\sum_i U_{real}(r_i) + U_{reciprocal}(r_i) - U_{self}(r_i) \\ &= \frac{1}{2}\sum_{\mathbf{n}}{}' \sum_{i=1}^{N}\sum_{j=1}^{N} q_i q_j \frac{\mathrm{erfc}(\alpha|\mathbf{r}_j - \mathbf{r}_i + \mathbf{n}|)}{|\mathbf{r}_j - \mathbf{r}_i + \mathbf{n}|} \\ &+ \frac{2\pi}{L^3}\sum_{\mathbf{k}\neq\mathbf{0}}\sum_{i=1}^{N}\sum_{j=1}^{N} q_i q_j \exp[i\mathbf{k}\cdot(\mathbf{r}_j - \mathbf{r}_i)]\frac{\exp(\frac{-|\mathbf{k}|^2}{4\alpha^2})}{|\mathbf{k}|^2} \\ &- \frac{\alpha}{\pi^{1/2}}\sum_i^N q_i^2 \end{aligned} \tag{3.9}$$

where the prime in the sum over $\mathbf{n}$ implies $i \neq j$ when $\mathbf{n} = \mathbf{0}$, $\mathbf{n} = (i_x,i_y,i_z)L$ with $i_\alpha = 0, \pm 1, \pm 2...$, k are lattice vectors in reciprocal space, $\mathbf{r}_i$ is the position of particle i, q_i is the charge of particle i and N are the number of atoms. The parameter α is an arbitrary parameter which governs the relative convergence rates of the two main series. The last summation in equation (3.9) is a self-correction term.

The advantage with this approach is that the energy can be calculated accurately by including relatively few of the terms in the summations in equation (3.9). This is due to the fact that the sum in real space and the one in reciprocal space fall off rapidly with increasing $|\mathbf{r}_j - \mathbf{r}_i|$ and $|\mathbf{k}|$ respectively.

3.4 Radial distribution function

The radial distribution function $g(r)$ describes how, on average, the distances between atoms in a system are distributed. $g(r)$ contains information about the crystal structure and can be obtained from for example neutron scattering or x-ray scattering experiments [10] [13].

The average number of atoms inside a shell of width δr at distance r from a fixed atom is denoted $n(r)$. This is averaged by using all atoms as the fixed point and calculating $n(r)$ for each one of them. The number density $\frac{N}{V}$ times the shell volume $4\pi r^2\delta r$ is the number of atoms inside the shell expected if the atoms were uniformly distributed. The ratio between $n(r)$ and the expected number of atoms is called the radial distribution function $g(r)$ and is hence given by

$$g(r) = \frac{V}{N 4\pi r^2 \delta r}\langle n(r)\rangle \tag{3.10}$$

where $\langle ...\rangle$ denotes an ensemble average.

For an ideal crystal $g(r)$ contains infinitely high peaks at certain characteristic distances depending on the crystal structure. For an ideal gas where atoms are moving around randomly, by construction, $g(r) \approx 1$ is expected.

3.5 Mean square displacement

The mean square displacement, MSD, describes the diffusion of atoms in a system and is defined as

$$\text{MSD}(t) = \frac{1}{N}\sum_{i=1}^{N}\langle|\mathbf{r}_i(t) - \mathbf{r}_i(0)|^2\rangle \tag{3.11}$$

where $\langle ...\rangle$ denotes an ensemble average and $\mathbf{r}_i(t)$ is the position of atom i at time t.

For gases and liquids the MSD will grow as a function of time and can be used to calculate the diffusion constant D according to

$$D = \lim_{t\to\infty}\frac{1}{6t}\text{MSD}(t) \tag{3.12}$$

For solids however the MSD goes towards a constant value as t increases due to atoms not moving freely in the system but fluctuating around their lattice position. This constant value will be called MSD_∞ for the rest of the report and is computationally computed as

$$\text{MSD}_\infty = \frac{1}{N_t - N_\tau}\sum_{n=N_\tau}^{N_t}\text{MSD}(n\cdot dt) \tag{3.13}$$

where N_t is the total number of timesteps and dt is the timestep. The correlation time is defined as $\tau = N_\tau \cdot dt$ and is the time it takes for the system to become uncorrelated i.e the time it takes for the system to "forget" its initial state.

3.6 Harmonic oscillator

In this section the harmonic oscillator in three dimensions is reviewed in order to be able to compare the obtained $\text{MSD}(t)$ and MSD_∞ in this study with results from a known system.

The harmonic oscillator in three dimension can be seen as a three independent one dimensional oscillators. The equation of motion for a harmonic oscillator in 1D is described by

$$m\ddot{x}(t) = -kx(t) \tag{3.14}$$

where k is a force constant. Assuming $x(0) = 0$ the solution is then given by

$$x(t) = A\sin(\omega t) \tag{3.15}$$

where A is the amplitude and $\omega = \sqrt{\frac{k}{m}}$ is the angular frequency of the oscillation. The period time is $t_p = \frac{2\pi}{\omega}$. The mean square displacement is calculated according to equation (3.11) as

$$\mathrm{MSD}(t) = \frac{1}{t_p}\int_0^{t_p}(x(t+s) - x(t))^2 ds = A^2(1 - \cos(\omega t)) \tag{3.16}$$

and then MSD_∞, according to equation (3.13) can be calculated as

$$\mathrm{MSD}_\infty = \lim_{t_p\to\infty}\frac{1}{t_p}\int_0^{t_p}\mathrm{MSD}(t) = A^2 \tag{3.17}$$

The total energy of the system is given by

$$U = \frac{1}{2}kA^2 = \frac{1}{2}k\mathrm{MSD}_\infty = \frac{1}{2}k_BT \tag{3.18}$$

where the equipartition theorem has been used for the last equality.

For a three dimensional harmonic oscillator there is three degrees of freedom, the energy is therefore three times as big and thus the following relation is obtained

$$\mathrm{MSD}_\infty = \frac{3k_b}{m\omega^2}T \tag{3.19}$$

where MSD_∞ now is calculated in three dimensions.

3.7 Intermediate scattering function

Often in crystal-scattering-experiments spatial correlations, such as $g(r)$, are not directly obtained but instead correlation functions in reciprocal space are the ones measured. One such function is the intermediate scattering function which can be measured by neutron spin echo spectroscopy.

The intermediate scattering function $F(\mathbf{k},t)$ is defined as

$$F(\mathbf{k},t) = \frac{1}{N}\sum_{n=1}^{N}\sum_{m=1}^{N}\langle e^{i\mathbf{k}\cdot(\mathbf{r}_n(t)-\mathbf{r}_\mathbf{m}(0))}\rangle \tag{3.20}$$

where $\mathbf{k}$ is a reciprocal vector. The self part of $F(\mathbf{k},t)$, when $n{=}m$, is called the self-intermediate scattering function and defined as

$$F_s(\mathbf{k},t) = \frac{1}{N}\sum_{n=1}^{N}\left\langle e^{i\mathbf{k}\cdot(\mathbf{r}_n(t)-\mathbf{r}_n(0))}\right\rangle \tag{3.21}$$

$F_s(\mathbf{k},t)$ will be unity for $t = 0$, and as t grows $F_s(\mathbf{k},t)$ will decreases due to $|\mathbf{r}_n(t)-\mathbf{r}_n(0)|$ growing. It is possible to average $F_s(\mathbf{k},t)$ over the direction of $\mathbf{k}$ and thus obtain $F_s(k,t)$ with $k = |\mathbf{k}|$.

There is a strong correlation between the self-intermediate scattering function and the mean square displacement. Assuming atoms fluctuate around their equilibrium position independently the following relation can be found

$$F_s(\mathbf{k},t) = 1 - \frac{1}{6}\mathrm{MSD}(t)|\mathbf{k}|^2 \tag{3.22}$$

For the full derivation of this expression refer to *Introduction to Solid State Physics* by Charles Kittel [13].

4

Computational methods

This project was carried out by running computer simulations. Phonon spectra was calculated using Pysic (Pythonic simulatin code), an object based calculator for atomistic many-body interactions [14]. Molecular dynamics simulations was performed using LAMMPS (Large-scale Atomic/Molecular Massively Parallel Simulator) on the computer cluster Beda at Chalmers Centre for Computational Science and Engineering (C3SE) provided by the Swedish National Infrastructure for Computing (SNIC). Some analysis of the output from LAMMPS was done using MATLAB and the python-distutils program dynsf. All figures was created with MATLAB.

In the following sections the computational methods are described in more detail.

4.1 Modelling $BaZrO_3$

As mentioned in the introduction the intention of this study was to find three different types of simple models for barium zirconate, one giving rise to an ordinary cubic structure, one giving rise to distortion and one intermediate on the limit between the two others. In order to distinguish them from each other in an easy way they are called model A (stable), model B (intermediate) and model C (unstable) throughout the report.

For simplicity a pair potential, described in section 3.2, was used for the models. In previous studies it has been shown that it is sufficient to take three types of interactions into account, Pauli repulsion, van der Waals interaction and Coulomb interaction [15]. The Buckingham potential were used to describe the Pauli repulsion and the van der Waals interaction, adding Coulombs law one arrives at

Table 4.1: Parameters in the Buckingham potential which previous studies have shown to be suitable for $BaZrO_3$ [15] [16]. These parameters were chosen as the ordinary potential (model A) since they give rise to no distortion.

Interaction	A(eV)	ρ(Å)	C(eVÅ^6)
Ba^{2+} – Ba^{2+}	0.000	0.0000	0.000
Ba^{2+} – Zr^{4+}	0.000	0.0000	0.000
Ba^{2+} – O^{2-}	931.700	0.3949	0.000
Zr^{4+} – Zr^{4+}	0.000	0.0000	0.000
Zr^{4+} – O^{2-}	985.869	0.3760	0.000
O^{2-} — O^{2-}	22764.300	0.1490	27.890

$$U(r_{ij}) = A_{ij}e^{-r_{ij}/\rho_{ij}} - \frac{C_{ij}}{r_{ij}^6} + \frac{q_i q_j}{r_{ij}} \tag{4.1}$$

Equation (4.1) is the form used to obtain all the three models with different properties, i.e. the difference lies in the parameters. As a starting point the parameters given in table 4.1 were used. These parameters have been found to be suitable values in previous studies of $BaZrO_3$ [15] [16]. In this project they were found to not give rise to distortion and were thus chosen as one of the three models, called model A.

As mentioned in chapter 2 a rough estimate of the stability of a perovskite structure is given by the Goldschmidt tolerance factor t. The tolerance factor t is defined by equation (4.2) where r_A, r_B are ionic radii for the cations respectively and r_X are the ionic radius for the anion. An undistorted perovskite ideally corresponds to $t = 1$ while lower values make distortion of the oxygen octahedra plausible.

$$t = \frac{r_A + r_X}{\sqrt{2}(r_B + r_X)} \tag{4.2}$$

To obtain a model that gives rise to distortion of the oxygen octahedra, starting from the stable model A , the obvious method is thus to try to increase $r_B + r_X$, in this case $r_{\mathrm{Zr}} + r_{\mathrm{O}}$, or decrease $r_A + r_X$, in this case $r_{\mathrm{Ba}} + r_{\mathrm{O}}$, or to do a combination of both. Since $r_{\mathrm{Ba}} + r_{\mathrm{O}}$ is coupled to the parameter ρ_{BaO} and $r_{\mathrm{Zr}} + r_{\mathrm{O}}$ is coupled to the parameter ρ_{ZrO} these were the parameters that were adjusted in order to decrease the tolerance factor and hence the stability of the perovskite structure. By studying the properties of the resulting potential when varying ρ_{BaO} and ρ_{ZrO} two additional models with desired properties were obtained and chosen as model B and C. The parameters for all three models are given in table 4.2.

The first two terms in the pair potential given by equation (4.1) are short ranged, i.e. they decay rapidly as r_{ij} grows, and are therefore negligible for large r_{ij}. This means

Table 4.2: The sets of parameter used in the Buckingham potential (first two terms of equation (4.1)) for the three types of potentials that were used. For all three cases $A_{\mathrm{BaO}} = 931.700\,\mathrm{eV}$, $A_{\mathrm{ZrO}} = 985.869\,\mathrm{eV}$, $A_{\mathrm{OO}} = 22764.300\,\mathrm{eV}$ and $C_{\mathrm{OO}} = 27.890\,\mathrm{eV\AA}^6$ were used with $A_{ij} = 0$ and $C_{ij} = 0$ for the remaining interaction. Model A do not give rise to distortion, model C give rise to significant distortion while model B is intermediate and give rise to a small distortion.

Model	ρ_{BaO} (Å)	ρ_{ZrO} (Å)
A	0.3949	0.3760
B	0.384	0.387
C	0.3820	0.3885

that a cut off r_{cut} can be used to reduce the computation time. The Coulombic term however is long ranged and can not be neglected for large r_{ij}. For a large number of charged particles this term becomes computationally expensive due to the amount of pairs i,j that contributes to the energy and therefore Ewald summation was used to speed up the simulations.

In a previous study where the parameters for model A was used, $r_{cut} = 6.0\,\mathrm{\AA}$ was chosen [16]. The potential energy per atom as a function of lattice constant a using $r_{cut} = 6.0\,\mathrm{\AA}$ is illustrated in figure 4.1 (left). As seen there is a clear jump in potential energy at about $a = 4.24\,\mathrm{\AA}$. This is explained by the fact that the distance between two atoms of the same type in next nearest unit cells is $\sqrt{2}a$ which becomes larger than r_{cut} for $a = 4.24\,\mathrm{\AA}$. The lattice constant for model A is $4.188\,\mathrm{\AA}$ however for a non-zero temperature atoms will move around and therefore the discontinuity may give rise to strange features. Also for model B and C as will be shown later the lattice constant will be slightly larger than $4.24\,\mathrm{\AA}$ which is why for all three models $r_{cut} = 12.0\,\mathrm{\AA}$, seen in figure 4.1 (right), was used.

Since the three models are relatively simple molecular dynamics simulations could be performed to study properties of the models.

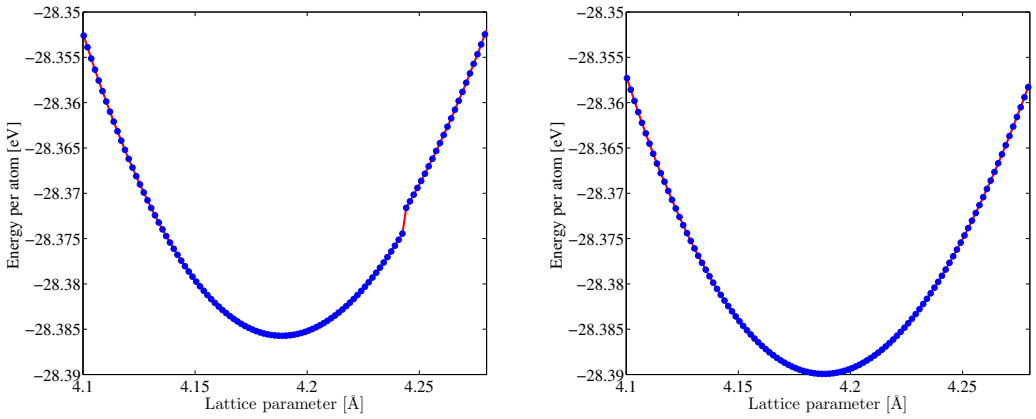

Figure 4.1: Energy per atom as a function of the lattice parameter, a, for the ideal cubic perovskite structure using model A with $r_{cut} = 6.0\,\text{Å}$ (left) and $r_{cut} = 12.0\,\text{Å}$ (right).

4.2 Molecular dynamics

Molecular dynamics is a classical method used to study the time evolution of many-particle systems using computer simulations. The method is classical in the sense that quantum effects are omitted and hence only classical mechanics are considered for the interactions of the particles to be studied. In general molecular dynamics is thus more suitable for heavy elements than for light elements such as hydrogen where quantum effects are important [17]. A brief description of the method follows below.

Consider N particles in a system where the interactions are described through an interatomic potential U, for example as the one given by equation (4.1). The forces acting on each particle is then given by

$$\mathbf{F_i} = -\nabla_i U(\mathbf{r}_1,...,\mathbf{r}_N) \tag{4.3}$$

where $\mathbf{r}_i$ is the position of particle i. The basic idea is, given some initial conditions $(\mathbf{r}_1(0),...,\mathbf{r}_N(0),\mathbf{v}_1(0),...,\mathbf{v}_N(0))$ at $t = 0$, then to for each particle numerically solve Newton's equation of motion (4.4)

$$m_i\ddot{\mathbf{r}}_i = \mathbf{F}_i \tag{4.4}$$

where $\ddot{\mathbf{r}}_i$ is the acceleration and m_i is the mass of particle i.

The trajectory of the particles, $(\mathbf{r}_1(t),...,\mathbf{r}_N(t),\mathbf{v}_1(t),...,\mathbf{v}_N(t))$, are obtained and are used to determine physical quantities. The Ergodic hypothesis, which states that an ensemble average is equivalent to a time average, is assumed to be true in order to compute ensemble averages. In this study the MD simulations were carried out in the NVT ensemble, meaning N,V and T were kept constant.

In order to run molecular dynamics at a constant temperature a thermostat is used meaning the equations of motion are modified in such a way that the velocities are rescaled to satisfy the equipartition theorem

$$T = \frac{2}{dNk_B} \sum_{i=1}^{N} \frac{1}{2} m_i v_i^2 \tag{4.5}$$

where k_B is the Boltzmann constant and d the dimension of the system. In this study the Nose-Hoover thermostat built into LAMMPS was used, a more detailed description can be found at the web page of the LAMMPS project [18].

The simulation box is a cuboid with dimensions L_x,L_y and L_z. For a bulk system periodic boundary conditions are often used in order to neglect boundary effects, which was the case in this study. This mean that the system is surrounded by replicas of itself. In order to avoid artificial behaviour such as particles interacting with itself or interacting with two images of the same atom the minimum image criterion states that $\frac{L_\alpha}{2} > r_{cut}$ must be satisfied for $\alpha = x,y,z$ [19].

4.3 Time averaging

As mentioned the Ergodic hypothesis is assumed to be true, i.e. ensemble averages can be calculated by calculating time averages.

Static quantities defined by an ensemble or time average, such as the radial distribution function, is computed as

$$\langle A \rangle = \frac{1}{N_t} \sum_{n=1}^{N_t} A(n \cdot dt) \tag{4.6}$$

where A is a static quantity and N_t is the number of timesteps. This is straightforward to calculate from the trajectories of particles, ($\mathbf{r}_1(t)$,...,$\mathbf{r}_N(t)$,$\mathbf{v}_1(t)$,...,$\mathbf{v}_N(t)$).

To compute dynamical properties defined by an ensemble or time average, such as the mean square displacement (MSD), equation (4.6) should however not be used. Instead moving averaging must be used and for example for the MSD for one particle one gets

$$\mathrm{MSD}(n \cdot dt) = \frac{1}{N_t - n} \sum_{m=1}^{N_t - n} |\mathbf{r}((n+m) \cdot dt) - \mathbf{r}(m \cdot t)|^2 \tag{4.7}$$

This means that the reference point $t = 0$ is shifted in order to compute the average.

4.4 LAMMPS

In this study the molecular dynamics simulations were carried out in the program LAMMPS (Large-scale Atomic/Molecular Massively Parallel Simulator), a freely-available open-source code. According to the website of the project "LAMMPS is a classical molecular dynamics code that models an ensemble of particles in a liquid, solid, or gaseous state. It can model atomic, polymeric, biological, metallic, granular, and coarse-grained systems using a variety of force fields and boundary conditions." [18].

LAMMPS has a number of different integrators, in this study the built in Velocity Verlet algorithm was used to numerically integrate the equations of motion. In addition the program has a lot of built in methods and features, but could also be extended if needed, making it possible to customise simulations. Due to LAMMPS being designed for parallel computing it is also well suited for being used on cluster-computers which were the case in this project.

Even though LAMMPS is a convenient tool for molecular dynamics simulations it can not perform sophisticated analyses or any visualisation of simulations. To do this the atomic trajectories are written as output data from LAMMPS and can then be processed by other softwares such as MATLAB and dynsf.

4.5 Dynsf

Dynsf is a python-distutils program for calculating the (partial) dynamical structure factor from a molecular dynamics simulation trajectory [20]. The program also calculates other crystal properties such as the intermediate scattering function. Since one type of input file that can be read by dynsf is LAMMPS-style trajectory output files the program was used to analyse the molecular dynamics simulations.

4.6 Simulation details

In this section the computational details of the simulations are provided. All molecular dynamics simulations were ran in the NVT ensemble, meaning the number of particles, temperature and volume were kept constant. For the molecular dynamics simulations a timestep of $dt = 0.002\,\text{ps}$ was chosen. The system was always initialized to a cubic perovskite structure. Before LAMMPS started to write output data the simulation was run for 200 000 timesteps, i.e. 400 ps, in order to equilibrate the system.

The radial cutoff for the potential was chosen, as described in section Modelling $BaZrO_3$, to be $r_{cut} = 12.0\,\text{Å}$. In order to fulfill the criteria $r_{cut} < \frac{L_i}{2}$, where $i = x,y,z$, the dimension of the system is always $L_x = L_y = L_z = 6$ unless else is specified. The

parameters for the ewald summation are automatically chosen in LAMMPS given a relative force accuracy which was set to 10^{-5} for all simulations.

5

Results

As mentioned in the introduction the intention of this study was to find three different types of simple potentials for barium zirconate, one giving rise to an ordinary cubic structure, one giving rise to distortion and one intermediate on the limit between the two others. Starting with the pair potential given by equation (3.8) three sets of parameters that meets this condition were obtained. For easy reference these parameters are presented in table 5.1 as model A (stable), model B (intermediate) and model C (unstable).

In the following sections results obtained for the three models are presented. Section 5.1 contains the lattice constants. In section 5.2 phonon spectra are presented together with a description of unstable modes found. The next section, 5.3, contains an investigation of the energy change when the atoms are moved along the unstable modes. All these are properties obtained from static calculations.

Table 5.1: The sets of parameter used in the Buckingham potential (equation (3.7)) for the three types of potentials that were used. For all three cases $A_{\mathrm{BaO}} = 931.700\,\mathrm{eV}$, $A_{\mathrm{ZrO}} = 985.869\,\mathrm{eV}$, $A_{\mathrm{OO}} = 22764.300\,\mathrm{eV}$ and $C_{\mathrm{OO}} = 27.890\,\mathrm{eV\mathring{A}}^6$ were used with $A_{ij} = 0$ and $C_{ij} = 0$ for the remaining interaction. Model A do not give rise to distortion, model C give rise to significant distortion while model B is intermediate and give rise to a small distortion. For a description of how these parameter were chosen see section 4.1.

Model	ρ_{BaO} (Å)	ρ_{ZrO} (Å)
A	0.3949	0.3760
B	0.384	0.387
C	0.3820	0.3885

Results from the molecular dynamics simulations are first presented in section 5.4 where the radial distribution function is investigated. Section 5.5 contains an analysis of the mean square displacement and in section 5.6 the self-intermediate scattering function is presented. Finally, in section 5.7, some results obtained using relatively large simulation volumes are presented.

5.1 Lattice constant

The energy of the undistorted perovskite structure as a function of lattice constant a for model A is presented in figure 5.1. The minimum is found at $a = 4.188\,\text{Å}$ which is in agreement with the result obtained by Stokes and Islam [15]. The same method is applied to model B and model C for which the lattice constant found is $a = 4.247\,\text{Å}$ and $a = 4.254\,\text{Å}$ respectively. These are the lattice constants used in the rest of the study, for convenience they are listed together in table 5.2.

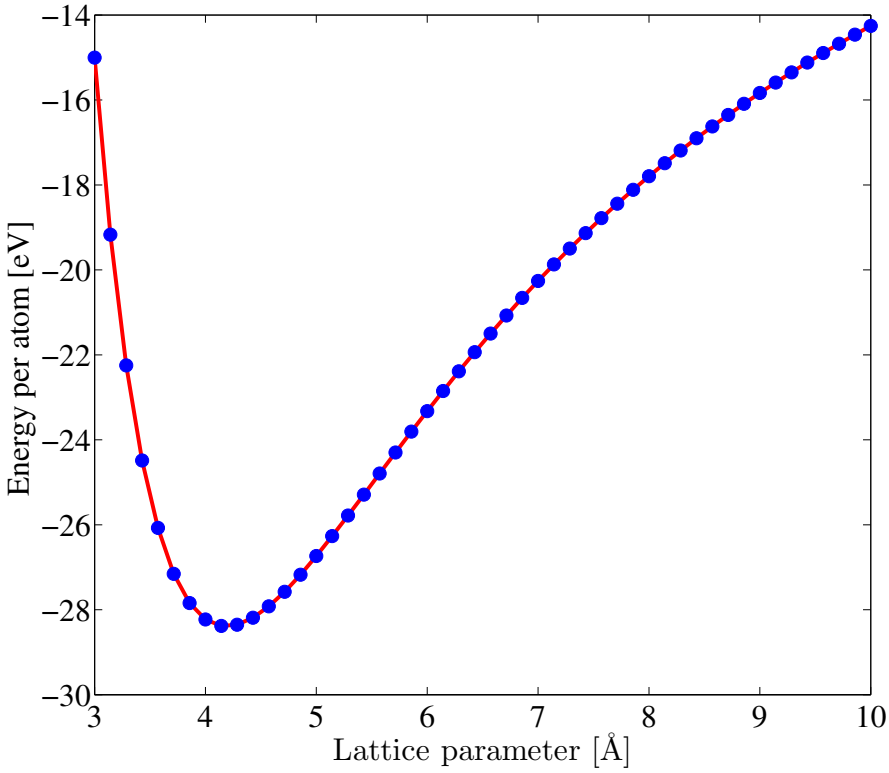

Figure 5.1: Energy per atom as a function of the lattice parameter, a, for the ideal cubic perovskite structure using model A.

Table 5.2: The lattice parameters obtained for the three models when the crystals are forced to be in an undistorted perovskite structure.

Model	Lattice parameter a (Å)
A	4.188
B	4.247
C	4.254

5.2 Phonon spectrum

In figure 5.2 the phonon spectrum obtained with the parameters for model A is illustrated. As seen there are no imaginary eigenfrequencies for these parameters and hence the energy is (at least locally) minimized for the undistorted perovskite structure. This means that the structure will be stable in time and no tilt will appear.

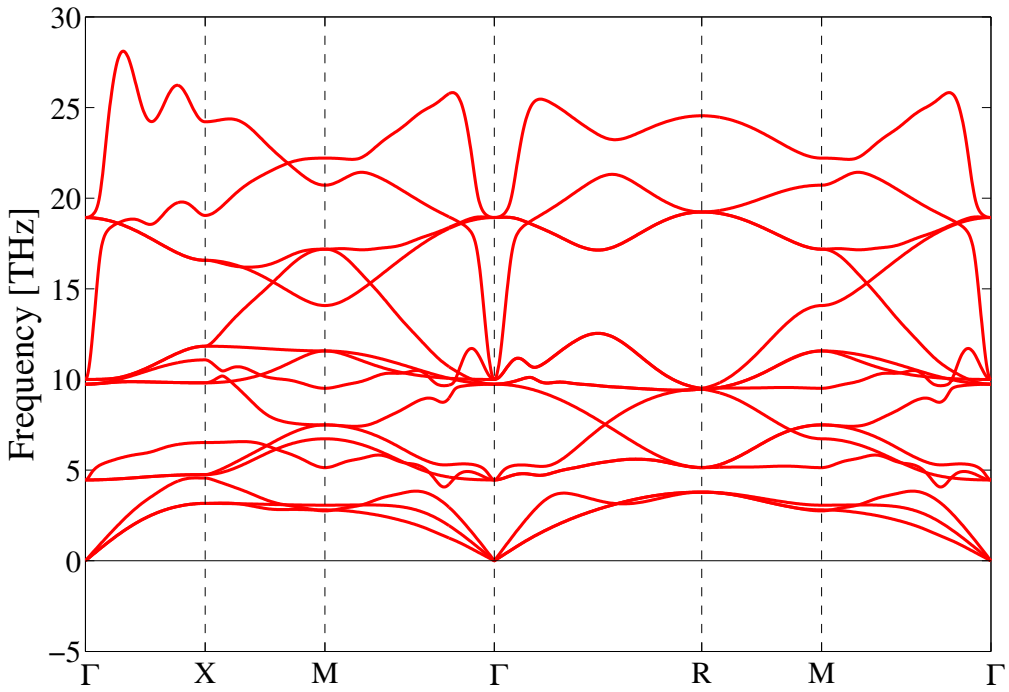

Figure 5.2: Phonon spectrum obtained using model A.

Figure 5.3 illustrates the phonon spectrum obtained with the Buckingham parameters for model C. The eigenfrequencies are clearly imaginary (illustrated as negative) at the M-point and the R-point. This indicates that the undistorted perovskite structure is not

stable in time and some kind of distortion will appear.

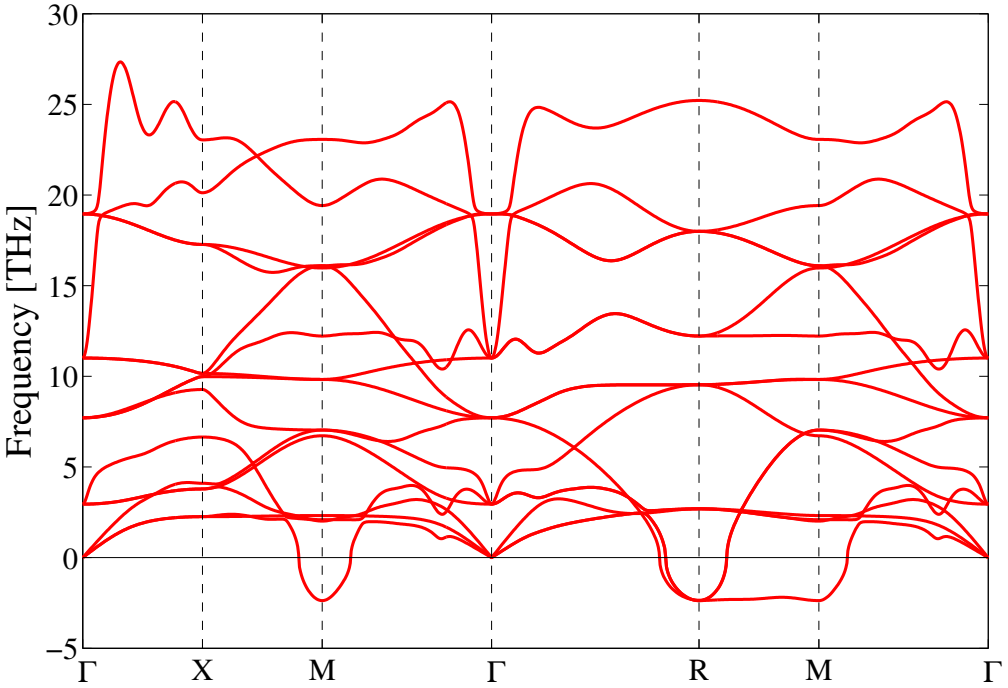

Figure 5.3: Phonon spectrum obtained using model C.

By studying the phonon spectrum for model C, illustrated in figure 5.3, in more detail one can note that there are three imaginary eigenfrequencies for the R-point and one for the M-point. The eigenmodes, **u**, corresponding to these eigenfrequencies are presented in table 5.3. The reason for the movement of barium and zirconium being omitted in table 5.3 is that they make only small movements compared with the oxygen atoms. One thus have that the four unstable modes corresponds to distortion of the oxygen atoms with the barium and zirconium atoms being approximatively fixed.

More precisely the obtained unstable modes corresponds to a rotation of the oxygen atoms in the unit cell around the zirconium atom together with a small increase in the distance between zirconium and oxygen atoms. Investigating the modes the corresponding Glazer notations for the four tilts are obtained to be $a^-b^-b^-$, $a^0b^-b^-$, $a^-a^-a^-$ and $a^0a^0c^+$ respectively, these are listed together with the associated modes in table 5.3.

Table 5.3: The unstable modes for model C together with the corresponding Glazer notation. The values are dimensionless constants indicating only the direction of the modes.

	R-point									M-point		
	$a^-b^-b^-$			$a^0b^-b^-$			$a^-a^-a^-$			$a^0a^0c^+$		
	O_1	O_2	O_3	O_1	O_2	O_3	O_1	O_2	O_3	O_1	O_2	O_3
x	0.5	0	-0.5	1	0	1	-1	0	1	0	0	-1
y	1	0.5	0	0	-1	0	1	-1	0	0	1	0
z	0	-0.5	-1	0	-1	0	0	1	-1	0	0	0

5.3 Distortion energy

To investigate the unstable modes the oxygen atoms are moved along the four modes in table 5.3 according to

$$\mathbf{r} = \mathbf{r}_{ideal} + d\mathbf{u}a \tag{5.1}$$

where $\mathbf{u}$ is a mode, $\mathbf{r}_{ideal}$ are the ideal cubic positions and d is a displacement factor. The energy as a function of d relative to the energy of the original perovskite structure ($d = 0$) can be seen in figures 5.4, 5.5 and 5.6 for model A, B and C respectively.

As expected from the phonon spectrum (figure 5.2), for model A the energy grows as a function of d. For model B however, small energy minima are found for the three R-point modes indicating that the system is not stable in the ideal cubic structure. The lowest energy of the three is for $a^-a^-a^-$ with a displacement factor of about $d = 0.009$. For model C the $a^-a^-a^-$ mode has the lowest minimum energy of the four unstable modes at about $-1.5\,\text{meV}$ for $d = 0.030$.

In figure 5.7 the movements of the oxygen atoms for the $a^-a^-a^-$ tilt in a perovskite structure is illustrated. Studying the structure the distortion is quite intuitive since the change of parameters compared to model A in principle corresponds to an increased radius for zirconium atoms and a decreased radius for barium atoms. The oxygen atoms is thus "pushed" out from its location in between two zirconium atoms toward one of the neighbouring barium atoms.

One can note that in figure 5.7 the three lower left oxygen atoms makes a movement around the zirconium atom at the lower left corner corresponding to a rotation vector $\vec{\omega} = (-1, -1,1)$ if the coordinate system are taken to be right-handed with the three oxygen atoms being situated in positive directions relative to the zirconium atom. This property of equal tilt about each of the three axes, together with the alternating rotation vector ($\pm\vec{\omega}$) in each direction, is what defines $a^-a^-a^-$.

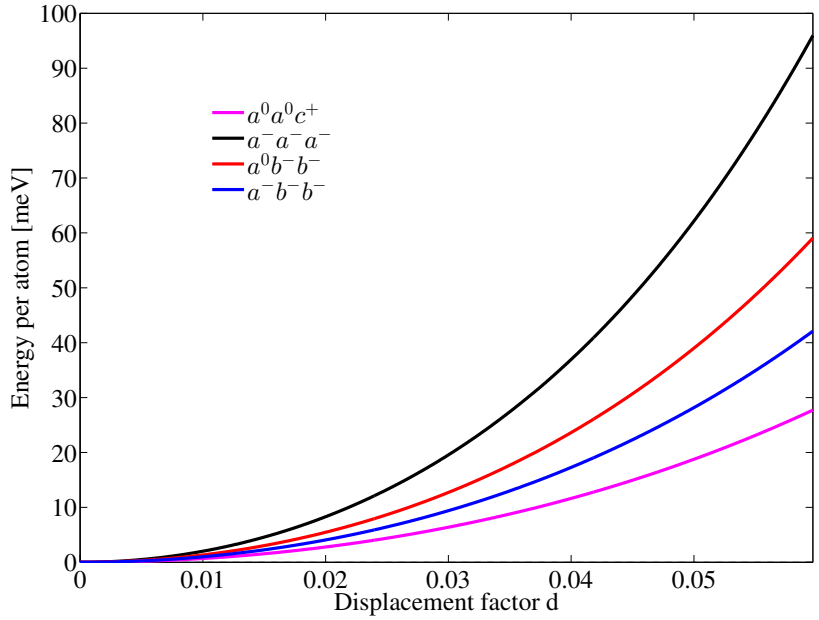

Figure 5.4: Energy per atom as a function of displacement factor d using model A for the four unstable modes described in table 5.3.

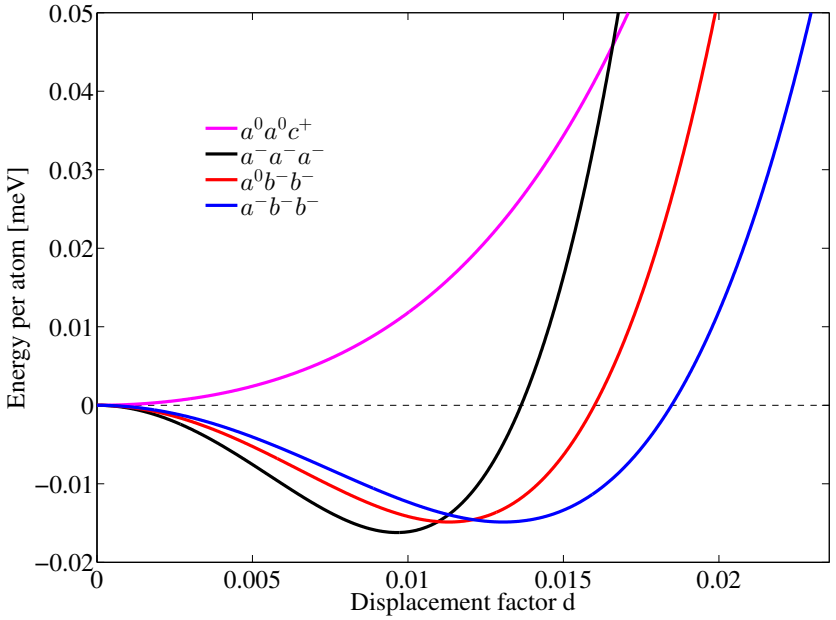

Figure 5.5: Energy per atom as a function of displacement factor d using model B for the four unstable modes described in table 5.3.

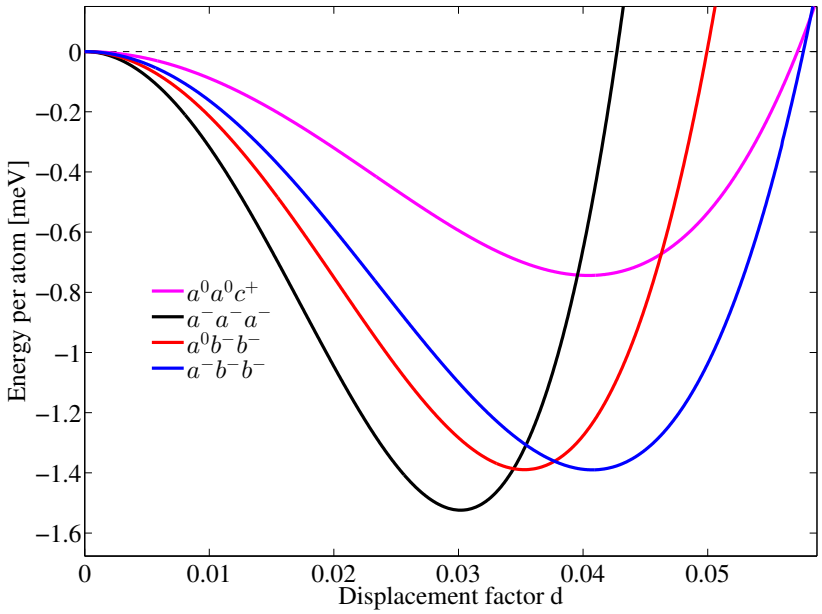

Figure 5.6: Energy per atom as a function of displacement factor d using model C for the four unstable modes described in table 5.3.

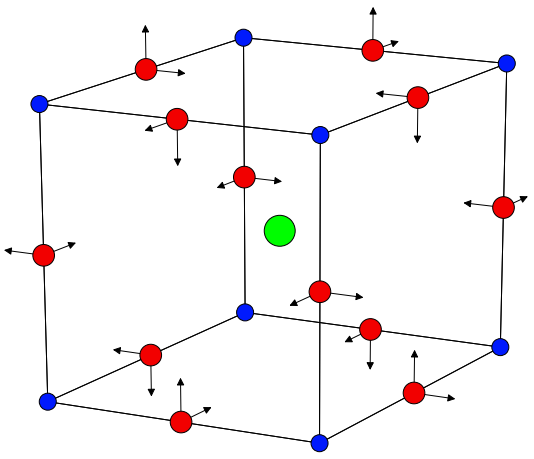

Figure 5.7: Schematic representation of the displacements of oxygen atoms for the $a^-a^-a^-$ rotation, where the arrows indicate the components of the movement for each atom. With the red circles being the oxygen atoms, blue being zirconium atoms and green barium atoms.

5.4 Radial distribution function

The ground state structure, i.e the structure with lowest energy, can be found using simulated annealing meaning starting the simulation at a high temperature and then gradually lowering it towards zero. From section 5.2 and 5.3 one have a good idea about the ground state structures for the models. For model A the ideal cubic perovskite structure is guessed to have the minimum energy while for model B and model C the $a^-a^-a^-$ structure seems to be the ground state.

The energy of the systems as a function of temperature as it approaches zero can be seen in figure 5.8. The dashed lines shows the energy of the minima in figures 5.4 5.5 and 5.6. As the temperature goes towards zero the energy of all three systems approaches their respective dashed line. This indicates that the undistorted cubic structure is in fact stable for model A while for model B and C the $a^-a^-a^-$ structure is the ground state.

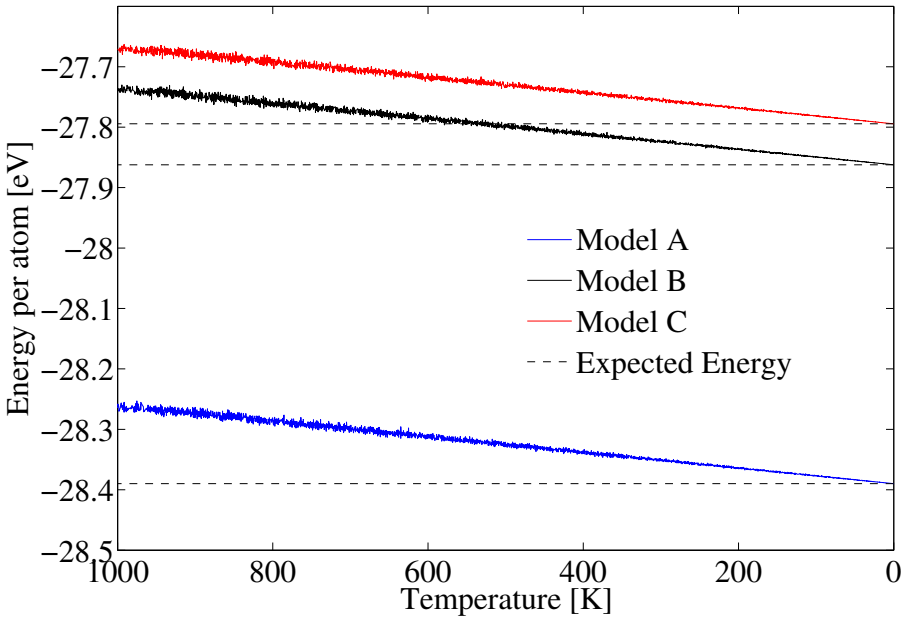

Figure 5.8: Energy as a function of temperature during simulated annealing for all three models. The dashed lines indicate the expected energies at $T = 0\,\mathrm{K}$.

To do further investigation the radial distribution function, $g(r)$, is computed for the oxygen atoms. The reason for excluding the other atoms is that they are, as mentioned, approximatively fix and hence the distortion is coupled to the oxygen atoms. Therefore both the temperature dependence and the different behaviours of the three models will be easy to distinguish in the radial distribution function for the oxygen atoms.

The expected ground state structures can be validated by comparing the radial distribution function, $g(r)$, after running simulated annealing with the corresponding expected $g(r)$ for the ground state structure. This comparison can be seen in figures 5.9, 5.10 and 5.11 for model A, B, and C respectively. The expected $g(r)$ for each model is obtained from a static computation with the atoms manually placed in the expected structure.

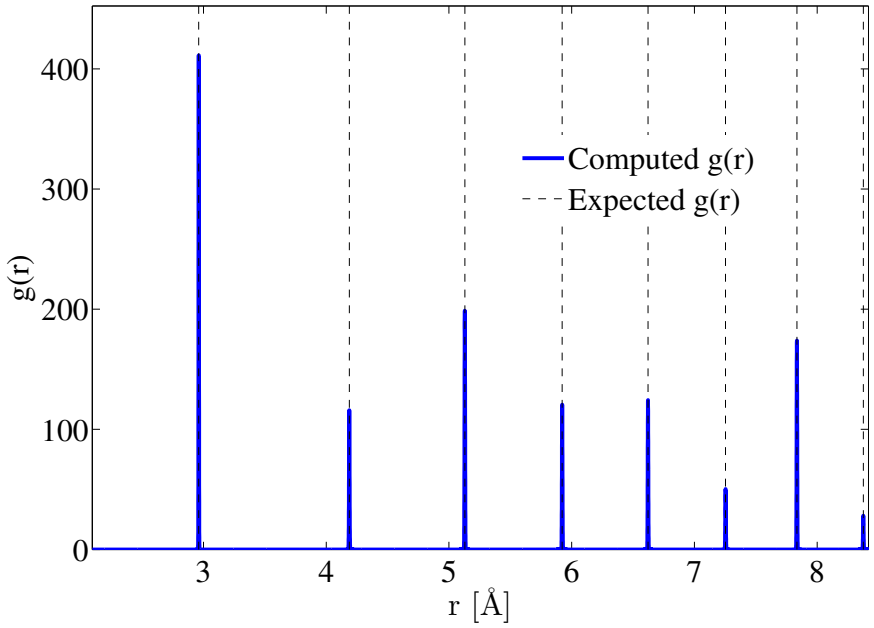

Figure 5.9: Radial distribution function $g(r)$ for model A after running simulated annealing. The dashed lines show where there would exists infinitely high peaks for the expected ground state structure, i.e. the undistorted cubic perovskite structure.

The computed $g(r)$ matches the expected $g(r)$ very well for all three models validating that the ground state for model A in fact is the ideal cubic structure while for model B and C the ground state is the $a^-a^-a^-$ structure.

The energy minimum for model B seen in figure 5.5 is only about $-0.02\,\text{meV}$ per atom. As seen in figure 5.10 when $T \to 0\,\text{K}$ the system does end up in the $a^-a^-a^-$ structure, but when the temperature is increased the kinetic energy of the atoms will become larger than $0.02\,\text{meV}$ meaning the structure will look more like an ideal cubic structure. This effect can be seen in figure 5.12 where $g(r)$ is shown for all three potentials at $T = 100\,\text{K}$.

All peaks in figure 5.12 are smoothen out compared to the $g(r)$ obtained by simulated annealing due to larger thermal fluctuations. The peaks for model B are noticeable lower compared to the ones for model A, due to the fact that model B is softer around the ideal cubic structure. The peaks for model C, as seen in figure 5.11, have also been smoothen

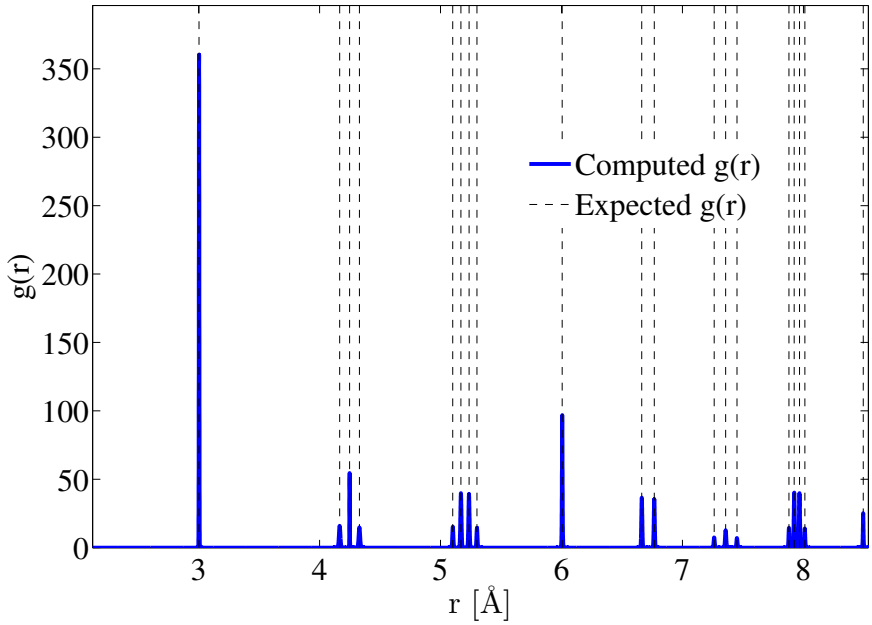

Figure 5.10: Radial distribution function $g(r)$ for model B after running simulated annealing. The dashed lines show where there would exists infinitely high peaks for the expected ground state structure, i.e. the $a^-a^-a^-$ structure.

out into a few wide ones. There is still however signs of the $a^-a^-a^-$ structure, most clearly seen from the double peaks where the other potentials have only one.

For $T = 300\,\mathrm{K}$ even model C shows cubic behaviour as is seen in figure 5.13. This shows that for large enough temperatures the energy barriers seen in figures 5.5 and 5.6 are negligible and the systems looks similar to model A. The temperature for which this transition in behaviour happens is strongly correlated with the height of the energy barrier.

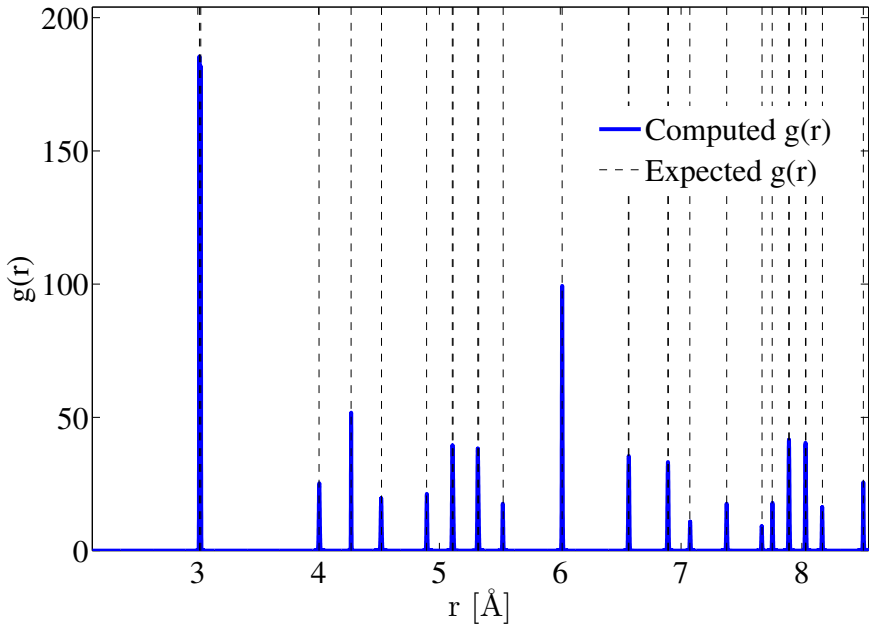

Figure 5.11: Radial distribution function $g(r)$ for model C after running simulated annealing. The dashed lines show where there would exists infinitely high peaks for the expected ground state structure, i.e. the $a^-a^-a^-$ structure.

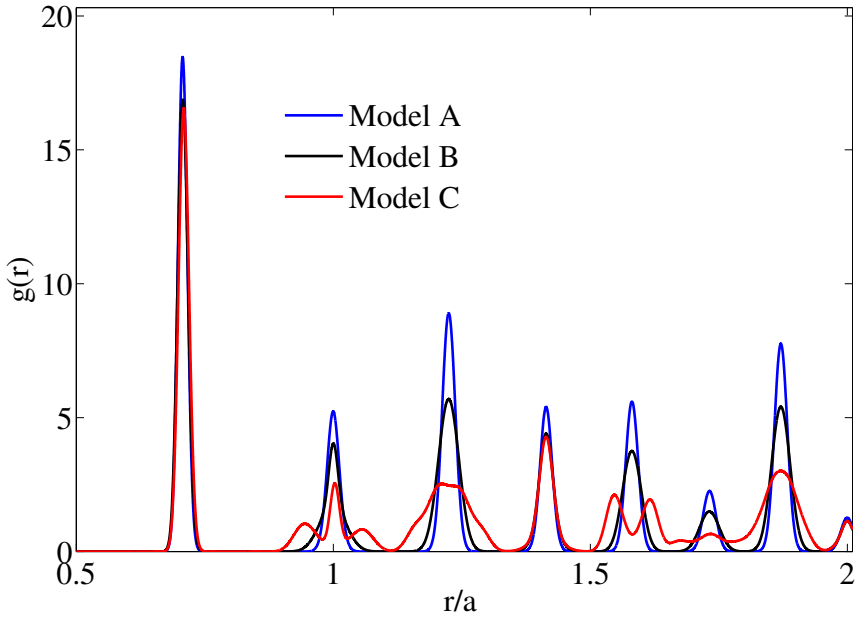

Figure 5.12: Radial distribution function $g(r)$ for all three model potentials at $T = 100\,\mathrm{K}$.

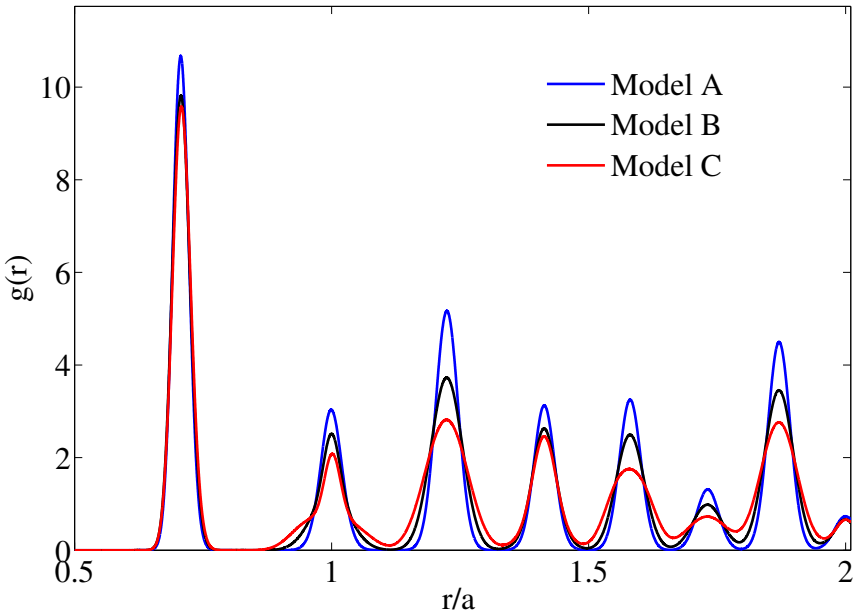

Figure 5.13: Radial distribution function $g(r)$ for all three model potentials at $T = 300\,\mathrm{K}$.

5.5 Mean square displacement

To further investigate the movement of the oxygen atoms, and how it differ between the three models, the mean square displacement of the oxygen atoms is studied.

In order to compute MSD_∞ according to equation (3.13) the correlation time, τ, must first be determined. In figure 5.14 the $\text{MSD}(t)$ is illustrated for the three models at $T = 130\,\text{K}$. The indicated τ shows a time for which all three plateaued. For simplicity this value will be used as correlation length for all three potentials for all temperatures. For low temperatures τ will become large because it will take longer time for the system to "forget" its initial state when the thermal fluctuations are small. It is also clear that τ is much larger for model C compared to the other two models. These problems will be discussed more later on.

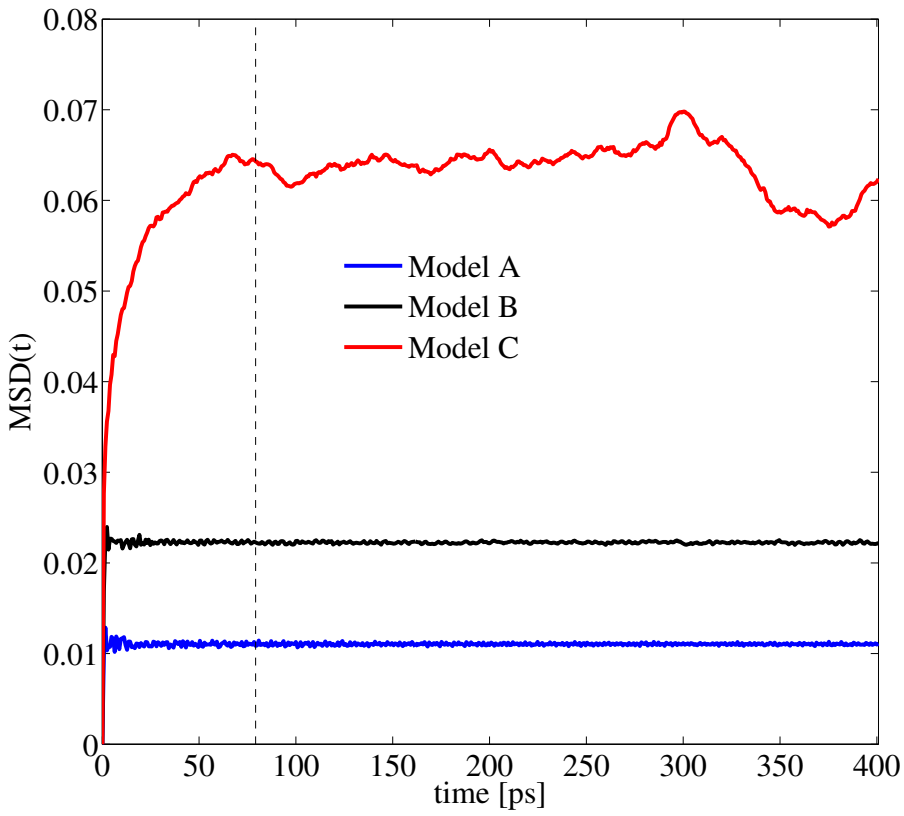

Figure 5.14: Mean square displacement as a function of time for the three potentials at $T = 130\,\text{K}$. The dashed line represent the correlation time τ for which the MSD for all three models have reached an equilibrium value.

The MSD_∞ is computed for many different temperatures and the result is presented in

figure 5.15. For model A the MSD_∞ grows linearly with temperature consistent with the behaviour of the harmonic oscillator. Using equation (3.19) the frequency is calculated to $f = 6.76\,\text{THz}$. This is in the range of the frequencies obtained in the phonon spectrum calculation (figure 5.2) and one can conclude that the oxygen atoms have the behaviour of a harmonic oscillator for model A.

The MSD_∞ for model C have a plateau for temperatures in the range of 60 K K to 200 K. The plateau comes from the fact that there is eight different orientations of the $a^-a^-a^-$ structure ($\vec{\omega} = (\pm 1, \pm 1, \pm 1)$). If the simulation is run long enough the probability of finding the system in any of the eight degenerated minima is uniform and approximately $\frac{1}{8}$ independently of the initial state. Assuming at $t = 0$ the system is oriented as $\vec{\omega}_1$, this means that the MSD_∞ will approximately approach the following constant

$$\text{MSD}_\infty \to \frac{1}{8} \sum_{i=1}^{8} d(\vec{\omega}_i, \vec{\omega}_1)^2 \tag{5.2}$$

where $d(\vec{\omega}_i, \vec{\omega}_1)$ is the distance between the oxygen atoms located in the $a^-a^-a^-$ structure oriented as $\vec{\omega_i}$ and $\vec{\omega_1}$. This constant value is calculated without regard to the contribution from small thermal fluctuations around the minima. For model C this value is computed to be about $0.066\,\text{Å}^2$ which matches well with the plateau seen in figure 5.15. After the plateau at about 300 K the MSD_∞ starts to grow linear with temperature indicating a harmonic oscillator behaviour. Just like for the radial distribution function for model C at higher temperatures the system seems to behave as a perfect cubic perovskite.

For model B no plateau can be seen, the calculated value using equation (5.2) is $0.0067\,\text{Å}^2$ which is too small to be seen. However investigating lower temperatures a plateau is found at about $0.0067\,\text{Å}^2$ as seen in figure 5.16. Note in this figure that the MSD_∞ for model C shows no signs of plateau value and instead behaves similarly to model A.

To better understand the low temperature behaviour of the MSD_∞ the standard deviation of the $\text{MSD}(t)$ for $t > \tau$ is computed and can be seen in figure 5.17. For model A and B the standard deviation indicates that the $\text{MSD}(t)$ have reached an equilibrium value. The large values of the standard deviation for models C at temperatures around 50 K to 150 K indicates that for these temperatures τ was too small. This means that the system, due to its relatively high energy barrier at about 1.5 meV, does not change between the different $a^-a^-a^-$ states enough during the simulation to make the distribution uniform. The condition for equation (5.2) is thus not satisfied.

Even for small temperatures such as 5 K model B reaches its plateau. This is due to the fact that its energy barrier between different $a^-a^-a^-$ states is only about 0.02 meV (as seen in figure 5.5) which is still small compared to the kinetic energy atoms have at $T = 5\,\text{K}$. This explains why the relaxation time for model B compared to model C is on a different timescale, as seen in figure 5.14.

For the temperatures below 50 K the standard deviation is small for model C because

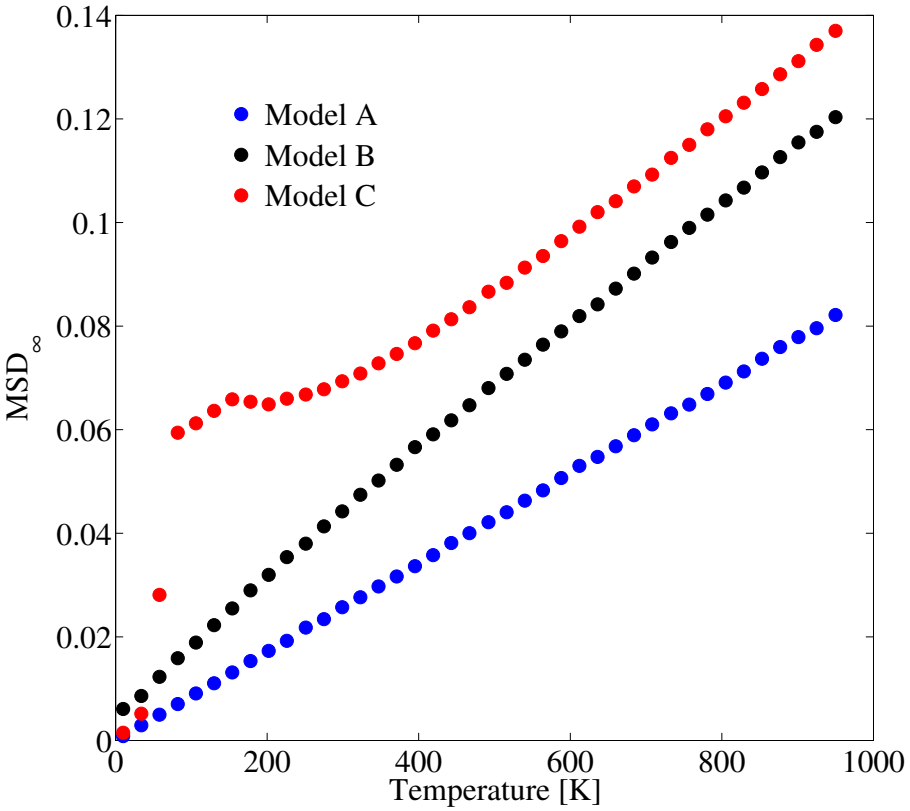

Figure 5.15: MSD_∞ as a function of temperature for the three models.

the system have never jumped to a different $a^- a^- a^-$ state as can be seen by the low value of the MSD_∞ in figure 5.16. Even for low temperatures if the total simulation time and τ are large enough the MSD_∞ for model C is expected to reach the plateau.

For $T = 60\,\mathrm{K}$ the MSD_∞ for model C did not reach its equilibrium value, as seen in figure 5.15. If the simulation is ran much longer, as seen in figure 5.18, the $\mathrm{MSD}(t)$ does reach the expected value of about $0.066\,\mathrm{\AA}^2$.

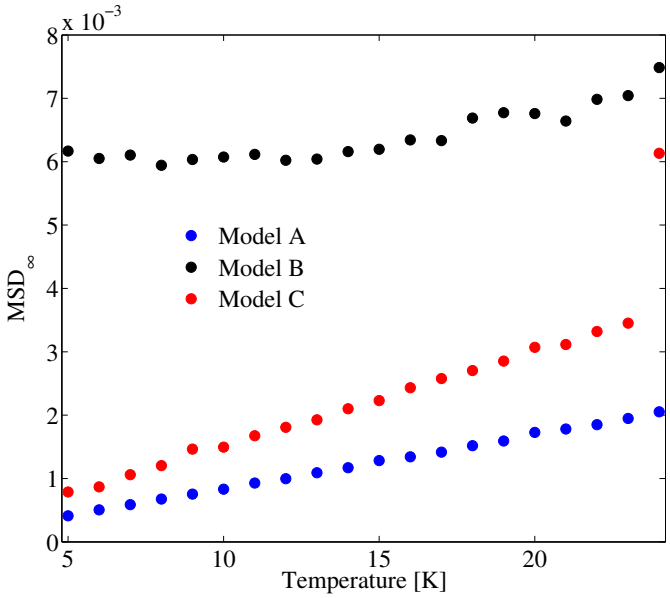

Figure 5.16: MSD_∞ as a function of low temperatures for the three models.

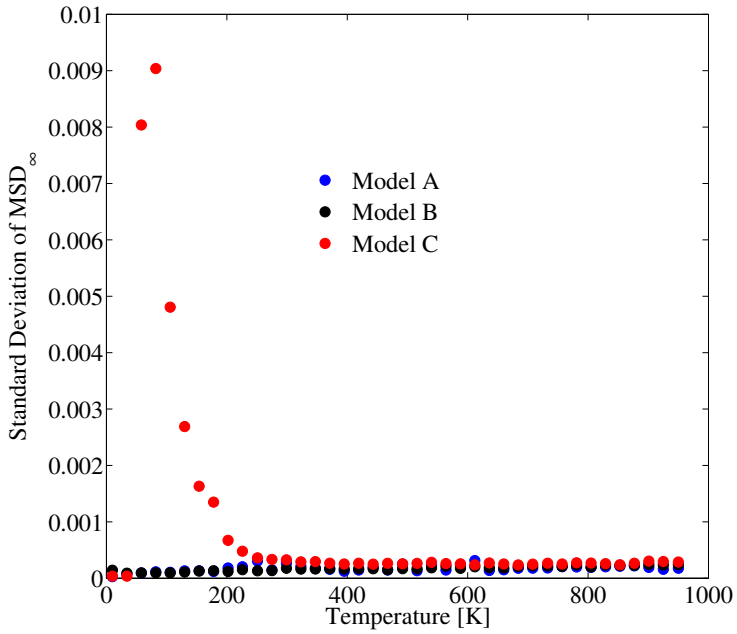

Figure 5.17: Standard deviation of MSD(t) as a function of temperature for the three models.

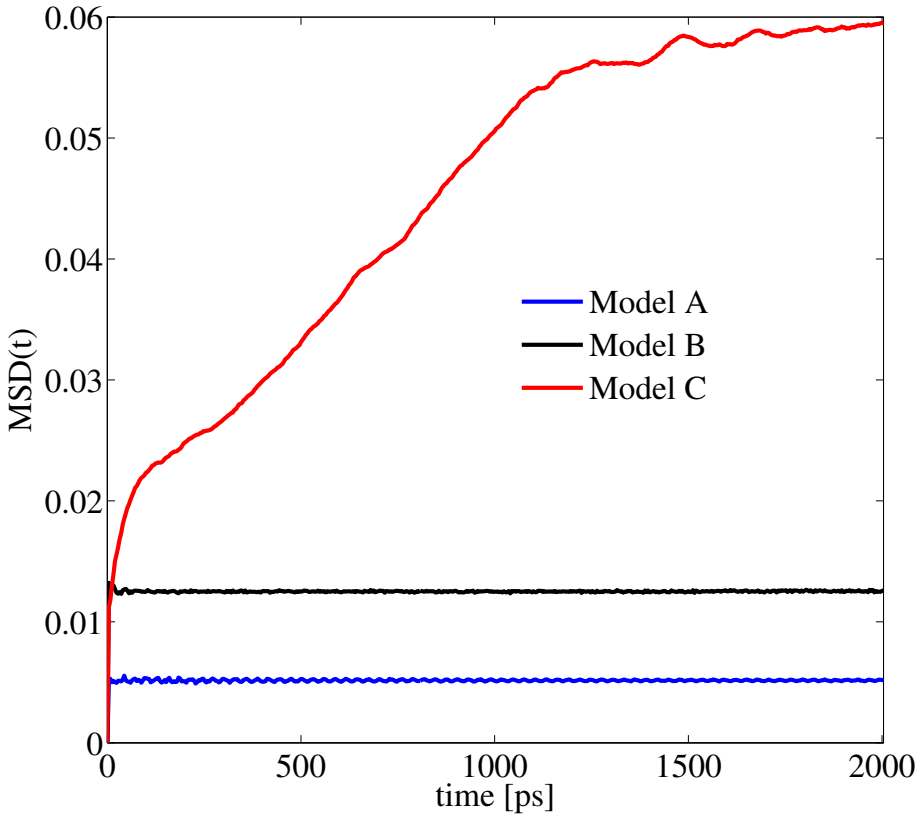

Figure 5.18: Mean square displacement, MSD(t), as a function of time for all three models at $T = 60\,\mathrm{K}$.

5.6 Self-intermediate scattering function

Neither the radial distribution function nor the mean square displacement can be directly measured in experiments but must instead be calculated from other quantities. One such quantity is the self-intermediate scattering function which is highly correlated to the mean square displacement as is discussed in the theory chapter (section 3.7).

The self-intermediate scattering function $F_s(k,t)$ for oxygen atom is computed. It is illustrated in figure 5.19 for model A, B and C at temperature 130 K for roughly the same k-value. In the previous section it was shown that the mean square displacement for model A behaves very similar to a harmonic oscillator with frequency $f = 6.76$ THz. Studying figure 5.19 the oscillation for model A has a period time of about 0.16 ps corresponding to $f = 6.25$ THz.

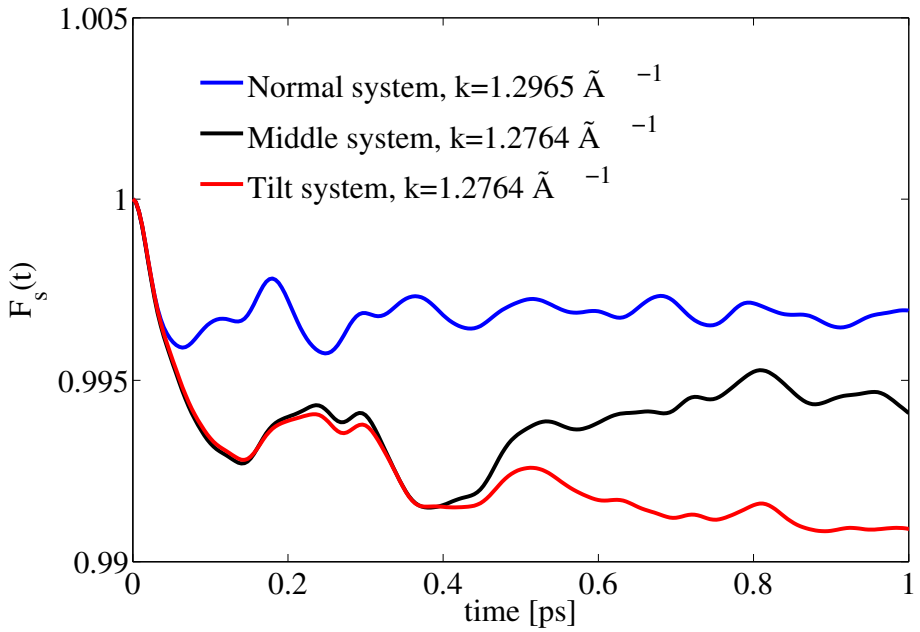

Figure 5.19: Self-intermediate scattering function $F_s(k,t)$ as a function of time for all three models at $T = 130$ K and roughly the same k value.

On a longer timescale the $F_s(k,t)$ is expected, like the MSD(t), to relax towards a finite value. This is seen in figure 5.20 for a temperature of 130 K. This is very similar to the mean square displacement in figure 5.14. Model C relaxes, as discussed in previous section, on completely different timescale compared to model A and B.

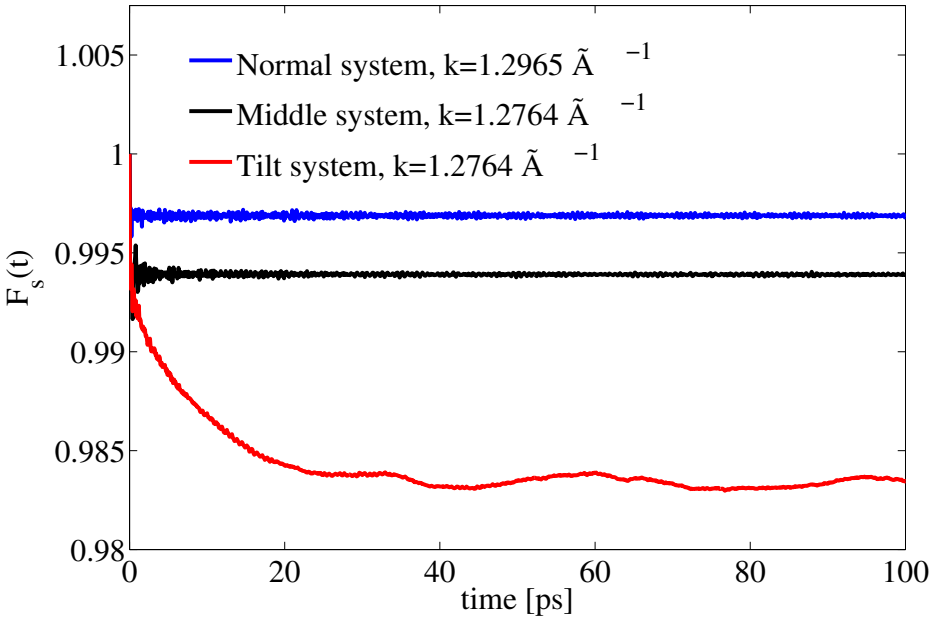

Figure 5.20: Self-intermediate scattering function $F_s(k,t)$ as a function of time for all three models at $T = 130\,\mathrm{K}$ and roughly the same k value.

5.7 Local ordering

To investigate local ordering and eventual formation of regions with different distortions simulations are performed for a significantly larger system size using model C. Ideally one would like to simulate a huge system but that would mean an immense amount of computation time, hence a trade-off between size and time is necessary. To get a relatively short computation time while still allowing different regions to occur a system of size 6x6x30 unit cells is first used. The advantage of using an elongated system is that the formation of different phases happens easier due to less interface energy.

If the atoms positions are averaged over a small period of time the thermal fluctuations will be neglected and it is possible to determine the "true" positions of the atoms. Doing this for the oxygen atoms in a unit cell it can then be identified to be in the $a^-a^-a^-$ structure oriented with a certain rotation vector $\vec{\omega}$. The identification process used for each unit cell is based on the angles of the displacement from the ideal perovskite structure for the oxygen atoms. For the results presented in this section simulations at low temperatures were used due to that the system may jump frequently between different $a^-a^-a^-$ phase for high temperatures. This would ruin the time averaging of the oxygen atoms positions.

For $T = 0\,\mathrm{K}$ the whole system is expected to be in the same $a^-a^-a^-$ phase. This is simply

due to the energy being lowest for this configuration and entropy having no impact. However as the temperature is increased formation of different $a^-a^-a^-$ phases may occur due to entropy contribution to the free energy. This is seen in figure 5.21 for $T = 70\,\mathrm{K}$ where each unit cell is color coded depending on its state. It is clear that two regions have been formed, one denoted with rotation vector $\vec{\omega} = (1,1,1)$ and the other with $\vec{\omega} = (1,1,-1)$. The same system is shown 20 ps later which indicates that the boundary between the two phases is moving around. Note that the rotation vector is alternating in all directions for each region and hence the region denoted $\vec{\omega} = (1,1,1)$ also consist of unit cells with rotation vector $\vec{\omega} = (-1,-1,-1)$. Similarly the region denoted $\vec{\omega} = (1,1,-1)$ also consists of cells with opposite rotation vector, i.e. $\vec{\omega} = (-1,-1,1)$.

For $T = 70\,\mathrm{K}$ almost all unit cells was identified to be in a $a^-a^-a^-$ state. The same system can be seen for $T = 120\,\mathrm{K}$ in figure 5.22. Here a lot more unidentified unit cells are seen, especially at the boundary between the two phases.

As expected the boundary between the regions are created so that the interface area is as small as possible. In order to understand these interfaces for a cubic system a simulation was run for 16x16x16 unit cells at $T = 30\,\mathrm{K}$. The result is shown in figure 5.23. This time four different $a^-a^-a^-$ phases are obtained, forming flat interfaces between each other. The formation of flat interfaces indicates that these have lower energy compared to curved interfaces.

The flat interfaces are partly formed due to the simulation dimension being even so that a "perfect" $a^-a^-a^-$ structure can be formed. In figure 5.24 a system of dimension 17x17x17 is seen for $T = 30\,\mathrm{K}$. Here all the eight different $a^-a^-a^-$ phases are shown by different colors. As mentioned the rotation vector is alternating in all directions for a $a^-a^-a^-$ distortion and hence in reality there are only four different types of phases. The regions with the same pair of rotation vectors are however displaced in such a way that if they had been in contact the interface would contain two successive unit cells with exactly the same rotation vector. That will not make one single $a^-a^-a^-$ region and hence these type of clusters are denoted as different phases.

An odd dimension size causes the flat regions such as those in figure 5.23 to become frustrated and therefore instead more sphere like regions are formed in figure 5.24. There is also no interfaces between the different $a^-a^-a^-$ states. The white part of the figure illustrates those unit cells that could not be identified as any of the eight $a^-a^-a^-$ phases. A preliminary study indicates that these white regions, that creates a bridge between the $a^-a^-a^-$ phases, consists of some of the other rotations with unstable modes, mainly a^0b-b-. This is due to the fact that all unstable modes are fairly close in energy and thus for larger system this kind of "glass" state may be found.

For the cubic system of size 16x16x16 in figure 5.23 only interfaces along the [100] directions have been formed. This is true for all simulations ran with an even sized system which may indicate that interfaces along other directions corresponds to a higher interface energy. The four-way intersections seen in figure 5.23 also indicates that the diagonal opposite phases may have a large interface energy compared to the other two

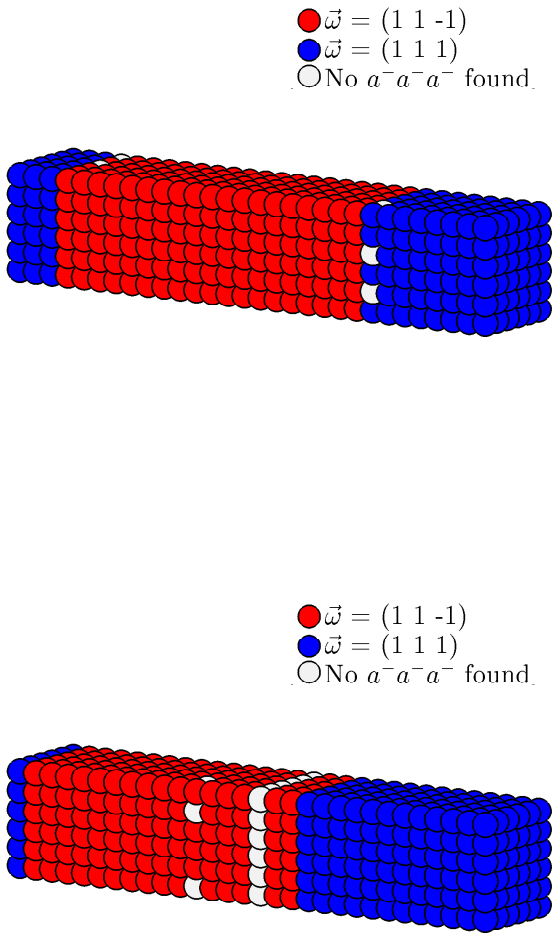

Figure 5.21: Each unit cell color coded according to which $a^-a^-a^-$ phase it is in for a system of $6x6x30$ unit cells at $T = 70\,\mathrm{K}$ using model C. The bottom figure shows the same system as the top but 20 ps later in the simulation.

phases.

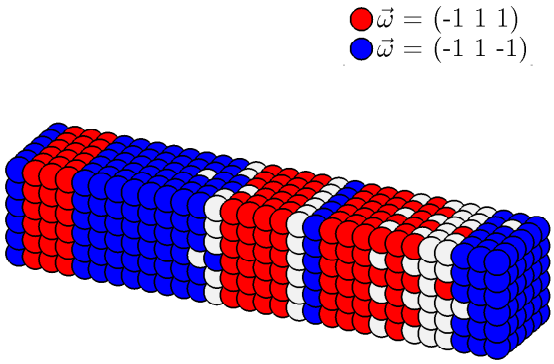

Figure 5.22: Each unit cell color coded according to which $a^-a^-a^-$ phase it is in for a system of $6x6x30$ unit cells at $T = 120\,\mathrm{K}$ using model C.

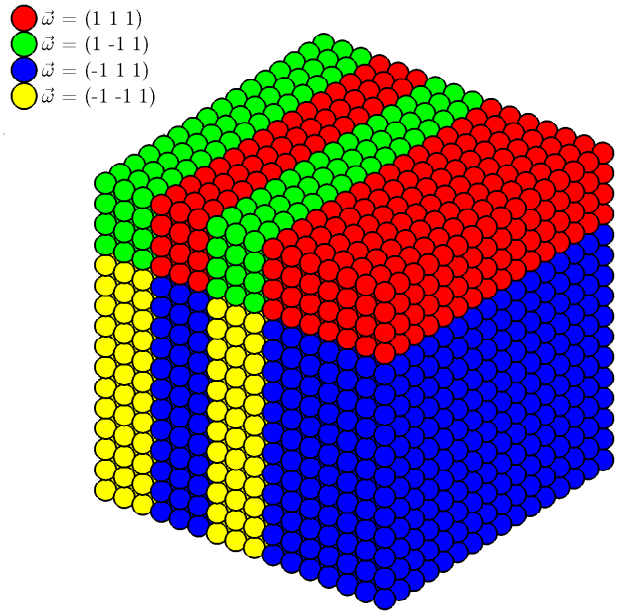

Figure 5.23: A system of size $16x16x16$ showing regions with different $a^-a^-a^-$ phases $T = 30\,\mathrm{K}$.

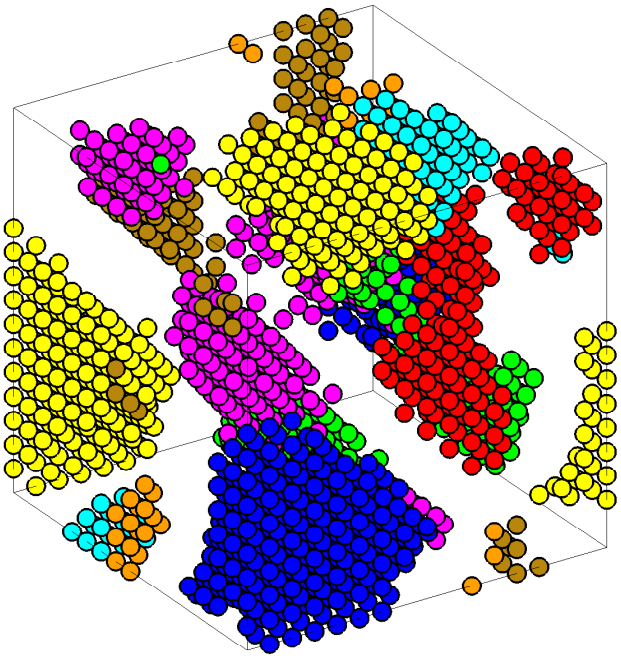

Figure 5.24: A system of size $17x17x17$ showing many regions with different $a^-a^-a^-$ phases for $T = 30\,\mathrm{K}$.

6

Discussion

In this study three different types of simple model potentials were found, one giving rise to an ordinary cubic structure, one giving rise to distortion and one intermediate on the limit between the two others. Although the models in this study are for barium zirconate ($BaZrO_3$) the principles are general and can easily be applied to whatever perovskite being of interest. Since the difference between the potentials for the three models lies in the parameters of the Buckingham potential one could in principle tune in the desired property for the model. This could be useful for perovskites in general and for perovskites known to be on the limit between stability and distortion, like barium zirconate, in particular. Using this kind of simple models physical quantities can be calculated and compared with experimental results to get an idea of whether a perovskite shows distortive behaviour or not.

Running simulated annealing down to $T = 0\,\mathrm{K}$ for all three models the expected ground state structures from the phonon calculations are found as seen in figure 5.8. However when molecular dynamics are run for $T = 300\,\mathrm{K}$ very similar structures are obtained seen in figure 5.13. This means that the system for model B and C is not fixed in the $a^-a^-a^-$ ground state but instead freely moves between all the eight degenerated $a^-a^-a^-$ structures and thus causing the time averaged $g(r)$ to look similar to model A.

From the MSD(t) in figure 5.14 its clear that model C behaves differently than the other two models for $T = 130\,\mathrm{K}$ due to the high energy barrier between the eight energy minima. In figure 5.15 the temperature dependence of the MSD_∞ is seen. For model C abnormally high values are found for low temperatures due to the jumping between the different groundstate structures.

For larger system at low temperatures regions of different $a^-a^-a^-$ phases are formed. This is caused by thermal fluctuations and the energy cost to change all unit cells to the

same phase. It takes a very long time for low temperatures to sample many different configurations which is why for each simulation different looking regions can be expected. As seen in figure 5.23 the four-way intersections indicate that interface energy between phases can vary. When a system of odd dimension (17x17x17) was used regions of different phases and shapes were formed seen in figure 5.24. Other distortions besides $a^-a^-a^-$ were also found and this sort of glass state is observed as discussed by Lebedev [5].

The identification of different $a^-a^-a^-$ phases used to investigate the large systems and formation of clusters is not in any way exact. The thermal fluctuation in fact makes it impossible to retrieve any sensible results if one is to characterize the individual cells at a specific time in an exact manner. To get around this the method used in this project was in principle to take short time averages of the positions and then determine the rotation vector $\vec{\omega}$ by checking the angles for the displacements of the oxygen atoms.

For perovskites known to have a relatively stable ideal perovskite structure the instability introduced by a change in ionic radii is still of interest. This is due to the interest in introducing dopants in perovskites to improve electrical properties, barium zirconate is for example often doped with yttrium to improve the proton conductivity. There could also be other defects in the material giving rise to distortion like for example oxygen vacancies.

Obviously one can study defects by performing a simulation with some atoms replaced with the specific defects. If the aim however is to just get a rough estimate of the possible distortion introduced by different defects it could be practical to apply the same method as was used in this study, i.e. change the ionic radii. Performing an experiment where the proportion of yttrium is increased from zero in barium zirconate it will not be surprising if the behaviour of the system makes a transition from that of model A to that of model C via model B.

In this study the distortion has been introduced in barium zirconate by changing parameters in a way that in principle corresponds to an increased radius for zirconium atoms and a decreased radius for barium atoms. The oxygen atoms is thus "pushed" out from its location in between two zirconium atoms toward one of the neighbouring barium atoms. With this in mind one can expect that distortion might also happen if the pressure is increased enough. In fact, as mentioned in section 2.2, in a recent experimental study a phase transition from cubic phase to tetragonal phase were found to take place at 17.2 GPa for barium zirconate [9].

The idea of the oxygen atoms being pushed out from its original position is also interesting in the context of density functional theory calculations. Using local-density approximation (LDA) the lattice constant is usually underestimated, i.e. the atoms are packed more tightly together than in the real structure. With generalized gradient approximation (GGA) the lattice constant is instead in general overestimated and the atoms are thus less densely packed. With this in mind one can suspect that LDA will more likely cause an oxygen instability compared with GGA. As mentioned in section

2.2 there is in fact different results for barium zirconate, LDA indicates instability while GGA calculations have found the ordinary perovskite structure to be stable. This is of course not just a matter of whether LDA or GGA is used but primarily depends on the material studied. Only for compounds on the limit between instability and stability, like barium zirconate, can one expect the significant difference in phonon spectra obtained with LDA compared to GGA.

Although it is useful due to its simplicity the three models in this thesis will, as mentioned, not be the best starting point if the intention is to make exact prediction about the properties of barium zirconate. For example the pair potential does not take into account directions of bonds, i.e. covalent bonds. In reality the atoms are also not perfectly ionic which for the pair potential partially can be taken into account by using real numbers for the ion charge.

Throughout this study the molecular dynamics was run in the NVT ensemble. The advantage of this ensemble is that it simplifies comparing the results of different models and temperatures due to the lattice constant being fixed. However in reality the material undergoes a thermal expansion meaning the lattice constant increases with temperature. There might also be a tendency for a distorted structure to decreases its lattice constant due to the structure being more closely packed. Furthermore a distorted structure may give rise to a rectangular cuboid system instead of maintaining the cubic structure.

A preliminary study using the NPT ensemble at zero pressure indicates that the lattice constant for model C does infact decreases with about 0.04 Å for 0 K. There was no indication of rectangular cuboid being formed which is probably due to the fact that the ground state $a^-a^-a^-$ is a symmetric distortion. For example for the unsymmetrical distortion $a^0a^0c^+$ the lattice constant may be different for the x, y and z directions respectively.

To fully explain the detailed features of both the short-range and long-range crystal structure in barium zirconate more studies are needed. Experimental research that could be compared with results obtained using computational modelling would be beneficial to further understand the material. For example one could perform total scattering techniques to investigate the local structure and inelastic neutron scattering to study dynamics on a local scale. In such a context the model potentials of this study could be used for comparison.

A development of the models in this study where yttrium can be include would be very interesting in order to understand the local ordering happening for Yttrium (Y) doped $BaZrO_3$. The locally increased ionic radii of part of the cations, due to Y being larger than Zr, may give rise to local or even global distortions. This could be studied for different concentrations of Y. Because barium zirconate is on the verge of stability it could also be interesting to introduce defects like oxygen vacancies in the material to understand their impact on the stability of the structure.

7

Conclusions

In this study three different types of simple models for barium zirconate ($BaZrO_3$) are found, one giving rise to an ordinary cubic structure, one giving rise to distortion and one intermediate on the limit between the two others. The stability of the models were investigated by calculating phonon spectra. Molecular dynamics were then used to study the time evolution of the system. The oxygen atoms for the model C were found to move a lot more compared to the other two models due to the potential being softer around the ideal cubic perovskite. The obtained radial distribution function indicates that the distortions are not found for temperatures above 300 K, meaning a phase transition have happend. Furthermore for large systems the formation of clusters of different distortions are observed.

A

Code example

To illustrate the kind of code used to obtain the results in the thesis a short example is included in this appendix. In case of further interest feel free to contact any of the authors.

A.1 LAMMPS example

Below a short LAMMPS script used to calculate the radial distribution function is presented. It consist of three main parts, reading the input file containing all information of the atoms, defining the potential wanted and lastly specifying the settings for molecular dynamics.

```
# ---------- Initialize Simulation ---------------------
clear
units metal
boundary p p p
atom_style full

# ---------- Create Atoms ----------------------
read_data ${name}_input.pos

# ---------- Define Interatomic Potential ---------------------

pair_style buck/coul/long ${Rcut}
pair_modify table 0
kspace_style ewald 1.0e-5
```

```
pair_coeff * * 0.0 0.1 0.0
pair_coeff 1 2 931.700 ${rho12} 0.0
pair_coeff 2 2 22764.300 0.1490 27.890
pair_coeff 2 3 985.869 ${rho23} 0.0

# ---------- Define Settings ---------------------

compute myRDF all rdf ${Nbins} 2 2

# ---------- Run MD ---------------------
reset_timestep 0
thermo 100
thermo_style custom step temp press lx

velocity all create $T 28459 rot yes dist gaussian mom yes
fix 1 all nvt temp $T $T 1

#Find equilibrium
timestep ${dt}
run ${tEq}

#Compute RDF
thermo 100
thermo_style custom step temp press lx

reset_timestep 0
fix 2 all ave/time ${Nevery} ${Nrepeat} ${tRun} &
 c_myRDF file RDF${name}.dat mode vector

run ${tRun}
```

Bibliography

[1] M. Johnsson, P. Lemmens, Crystallography and chemistry of perovskites.

[2] A. M. Glazer, The classification of tilted octahedra in perovskites, Acta Crystallographica Section B 28 (11) (1972) 3384–3392.

[3] L. Bellaiche, J. Íñiguez, Universal collaborative couplings between oxygen-octahedral rotations and antiferroelectric distortions in perovskites, Phys. Rev. B 88 (2013) 014104.

[4] W. Zhong, D. Vanderbilt, Competing structural instabilities in cubic perovskites, Physical Review Letters 74.

[5] A. I. Lebedev, I. A. Sluchinskaya, Structural instability in bazro3 crystals: Calculations and experiment.

[6] A. Bilic, J. D. Gale, Ground state structure of $bazro_3$: A comparative first-principles study, Physical Review B 79.

[7] A. R. Akbarzadeh, I. Kornev, C. Malibert, L. Bellaiche, J. M. Kiat, Combined theoretical and experimental study of the low-temperature properties of bazro3, Phys. Rev. B 72 (2005) 205104.

[8] F. Giannici, M. Shirpour, A. Longo, A. Martorana, R. Merkle, J. Maier, Long-range and short-range structure of proton-conducting y:bazro3, Chemistry of Materials 23 (11) (2011) 2994–3002.

[9] X. Yang, Q. Li, R. Liu, B. Liu, H. Zhang, S. Jiang, J. Liu, B. Zou, T. Cui, B. Liu, Structural phase transition of bazro3 under high pressure, Journal of Applied Physics 115 (12) (2014) –.

[10] E. Kaxiras, Atomic and Electronic Structure of Solids, 1st Edition, Cambridge University Press.

[11] D. Alfè, A program to calculate phonons using the small displacement method, `http://www.homepages.ucl.ac.uk/~ucfbdxa/phon/phon.html` (Apr. 2014).

[12] P. Gibbon, G. Sutmann, Long-range interactions in many-particle simulation, Quantum simulations of many-body systems: from theory to algorithm. Eds. J. Grotendorst, D. Marx and A. Muramatsu. NIC-series 10 (2002) 467–506.

[13] C. Kittel, Introduction to Solid State Physics, 8th Edition, Wiley, 2005.

[14] T. Hynninen, Pysic (pythonic simulation code), `http://thynnine.github.io/pysic/` (Feb. 2014).

[15] S. J. Stokes, M. S. Islam, Defect chemistry and proton-dopant association in $bazro_3$ and $bapro_3$, J. Mater. Chem. 20 (2010) 6258–6264.

[16] G. V. Lewis, C. R. A. Catlow, Potential models for ionic oxides, Journal of Physics C: Solid State Physics 18 (6) 1149.

[17] D. Frenkel, B. Smit, Understanding Molecular Simulation: From Algorithms to Applications, 1st Edition.

[18] Lammps molecular dynamics simulator, `http://lammps.sandia.gov/` (May 2014).

[19] J. Thijssen, Computational Physics, 2nd Edition.

[20] dynsf, tool for calculating dynamical structure factor, `https://code.google.com/p/dynsf/` (May 2014).